Joint Centre for Mesoscale Meteorology, Reading, UK

The sting at the end of the tail: damaging winds associated with extratropical cyclones. Part I: observational evidence and proposed mechanisms

JCMM Internal Report No 135

NWP Technical Report No 388

July 2002

K A Browning

Met Office Joint Centre for Mesoscale Meteorology Department of Meteorology
University of Reading PO Box 243 Reading RG6 6BB United Kingdom
Tel: +44 (0)118 931 8425 Fax: +44 (0)118 931 8791
www.metoffice.com

Designed and produced by the Met Office © Crown copyright 2001 01/0240 The Met Office logo is a registered trademark.

The sting at the end of the tail: damaging winds associated with extratropical cyclones. Part I: observational evidence and proposed mechanisms

By K.A. BROWNING*
University of Reading, UK

SUMMARY

Strong surface winds often accompany the low-level jets that occur along the cold fronts of extratropical cyclones, but there is evidence that the most damaging events occur in a distinctly different part of a certain class of cyclone. The most damaging extratropical cyclones go through an evolution that involves the formation of a bent-back front and cloud head separated from the main polar-front cloud band by a dry slot. When the cyclone attains its minimum central pressure, the trailing tip of the cloud head bounding the bent-back front forms a hook which encircles a seclusion of warm air. The most damaging winds occur near the tip of this hook – the sting at the end of the tail.

This paper presents observational studies of three cyclones. One of them, the Great Storm of October 1987 in south-east England, is re-examined on the mesoscale to show the close relationship between the damaging winds and the region where low-level cloud-head air interacts with recently-descended very dry air in the dry slot. It is well known that much of the development in explosively deepening cyclones is due to the release of latent heat during condensation. An extra dimension explored in this paper is the role of latent heat during evaporation in increasing the surface winds. Several hypotheses are developed relating to mesoscale processes that are believed to lead to local enhancement of the surface winds. Key processes include

*Corresponding author: Joint Centre for Mesoscale Meteorology, Department of Meteorology, University of Reading, PO Box 243, Reading, Berkshire, RG6 6BB, UK.

conditional symmetric instability leading to multiple slantwise convective circulations within the cloud head and the rapid evaporation of associated cloud material at the tip of the cloud head. Gravitational instability leading to convective showers in the dry slot plays a significant but secondary role.

1. INTRODUCTION

This paper is about the observed structure of an extreme class of rapidly deepening extra-tropical cyclone that produces a disproportionately large social and economic impact as a result of severe surface winds. Muir-Wood, in a lecture to the Royal Meteorological Society in December 2001, stated that the total insurance loss from such windstorms in Europe since 1985 was 24 billion Euro. Worldwide these European windstorms are second only to US hurricanes as a traded catastrophe risk. He pointed out that two extra-tropical cyclones – Lothan and Martin – occurring in NW Europe over Christmas 1999 (Pearce *et al.* 2001, Ulbrich *et al.* 2001), gave forestry losses that alone amounted to 3.4 billion Euro; they also left 3.5 million customers without electricity and up to 1 million without telephone lines. Other extratropical cyclones well known for the wind damage they inflicted include the 1979 Fastnet Storm (Pedgley 1997), the 1990 Burns' Day storm (McCallum 1990) and the 1997 Christmas Eve Storm (Young and Grahame 1999), as well as the Great Storm of October 1987 (see special issues of Weather (Vol.43, No.3) and Meteorological Magazine (Vol.117, No.1389)).

Coming from the perspective of global risk management, Muir-Wood derived a worst-case scenario in which a "Lothan storm" crosses London. He estimated a loss potential of up to £8 billion and 50 to 300 fatalities according to time of day and day of week. He drew attention to the poor quality of present-day forecasts of such extreme events: even 2 hours before Lothan hit Paris, windspeeds expected in the Paris area were being underestimated by 25%, equal to a 6 to 8-fold underestimate in damage. This underlines the need for improved prediction, and better prediction may require both better targeted observational input and better representation of processes within numerical weather prediction models. This can be achieved in part by gaining better understanding. Since the extent of the damaging winds is often quite

localized there may be a particular need for improved understanding of the small and mesoscale structures and mechanisms – hence the present study.

There is a large body of literature addressing the synoptic-scale structure of extra-tropical cyclones, henceforth cyclones for short – see the monographs edited by Newton and Holopainen (1990) and Shapiro and Grønås (1999). However, few studies have addressed the observed mesoscale structure of these cyclones and even fewer have addressed the mesoscale structure of cyclones that are extremely damaging or potentially so. Notable exceptions are some of the cyclones observed in ERICA (Experiment on Rapidly Intensifying Cyclones over the Atlantic) for which Neiman *et al.* (1990, 1993), Nieman & Shapiro (1993) and Wakimoto *et al.* (1995) presented detailed observations from special aircraft and other sources. Some of these observations formed the basis of the cyclone life-cycle model of Shapiro and Keyser (1990) which applies to many cyclones and particularly to the rapidly developing cyclones that produce the most damaging surface winds. The present author (1999, 2003), in two review articles, used the Shapiro-Keyser model as the framework within which to interpret various mesoscale and smaller-scale processes but the emphasis in these reviews was not on the damaging winds per se. The purpose of the present study, is to address the smaller-scale processes specifically with a view to ascertaining their effect on the surface winds.

It is well known that much of the development in rapidly deepening cyclones is due to the release of latent heat during condensation (Kuo and Reed 1988, Shutts 1990, Grønås 1995) An extra dimension explored in this paper is the role of latent heat sinks during evaporation in locally intensifying the surface winds. In section 2 we review some key published results to provide the dynamical context for the ensuing observational case studies. In section 3, we revisit the Great Storm of October 1987. Although this cyclone has been much studied on the larger scale, we find that there is more that can be learned from a detailed mesoanalysis of the many autographic charts that have been collected by the Met Office and kindly made available by M.J. Bader. In section 4, two recent cyclones that produced limited wind damage are considered briefly in order to support aspects of the analysis in section 3. One of the cyclones is analysed using model output but the primary thrust of

the paper is to establish structural characteristics observationally and to use these to derive hypotheses as to the mesoscale mechanisms that may be important in locally enhancing the surface winds. We focus on a specific part of the cyclone, close to and to the right of its centre, just downwind of a characteristic cloud signature, referred to as a hooked cloud head.

2. CONTEXT FOR THE DAMAGING WINDS

(a) Frontal fracture and the development of the cloud head and dry slot

A cloud head and dry slot are characteristic features of cyclones that produce damaging winds, and the most damaging winds are closely associated with them. We therefore start by reviewing some of the attributes of these features to provide a context for analysing and interpreting the strong-wind events. The cyclone life-cycle model of Shapiro and Keyser (1990), reproduced in Fig.1, shows the evolution of the cloud head as the cyclone develops. The cloud head becomes well defined at Stage III where it can be seen extending west- and north-westwards from the bent-back front. At this stage the main cold front and associated polar-front cloud band have advanced ahead of the cyclone centre leaving a region relatively free from cloud in between. This is called the dry slot. As the cyclone matures (Stage IV) the cold air in the dry slot encircles it, leading to a seclusion of warm air surrounded by the tail of the bent-back front and the associated tip of the cloud head. The present study will focus on the region near the end of the tail of the bent-back front, known to be a preferred site for damaging winds. Grønås (1995) recalls that "as a young forecaster in the late 1960's, (he) was informed that the strongest winds ever recorded in (Norway) have been linked to a (bent-back front). Such a structure has been called "the poisonous tail" of the bent-back front, after F. Spinnangr". We refer to the damaging winds in this region as the sting at the end of the tail.

(b) The hooked tail-end of the cloud head and associated cold conveyor belt

The diagram in Fig. 2, from Bader *et al.* (1995), shows the cyclone structure in terms of the conveyor-belt paradigm. The primary warm conveyor belt (W1) extends as a cloudy airstream along the main cold front before

rising above the warm front. Warm air in the secondary warm conveyor belt (W2) crosses the dry-slot region before rising above the bent-back front. The W2-flow fans out and forms the upper part of the cloud head. The cold conveyor belt occupies the lower part of the cloud head, including its southern tip where it begins to hook around the cyclone centre behind a secondary cold front. Dry-intrusion air, recently descended from upper levels, overruns the W2 air* ahead of the secondary cold front within the dry-slot region. Figure 3, also taken from Bader *et al.* (1995), shows the typical evolution of the hooked cloud head, extending around the cyclone centre as it evolves from the stage shown in Fig.2 to the final spiral structure (Fig.3(c)) which is characteristic of Stage IV in Fig.1. According to Bader *et al.*, by the time the hook has rotated to the forward side of the cyclone centre (Fig.3(b)), the cyclone will have reached its maximum development. At this stage the cyclone vortex is almost vertical.

(c) The creation of potential instability in the dry slot

As shown by Browning *et al.* (1996, 1997) and Griffiths *et al.* (2000), differential rotation with height around the cyclone vortex causes the 3-D configuration of the wet-bulb potential temperature θ_w-frontal surfaces to change in a characteristic way as the cyclone evolves (Fig.4). Initially (Fig.4(a)) the θ_w-front slopes backwards everywhere (ie it is an ana-front) but, as time progresses, a portion just south of the cyclone vortex corresponding to the dry-slot region acquires a forward slope, ie a kata-frontal structure. That is to say, low -θ_w air overruns higher-θ_w air as in the split-front model of Browning and Monk (1982). By the time the cyclone reaches the stage shown in Fig.2, the entire dry-slot region tends to be characterised by this kind of overrunning. The resulting potential instability leads to a few outbreaks of upright convection and showers in the dry slot (Carr and Millard 1985). A recent example is the series of arc rainbands analysed by Browning and Roberts (1999).

* Except where downdraughts from convective showers bring dry-intrusion air down to the surface, as in the case study in section 3.

(d) The existence of multiple stacked slantwise convective circulations in the cloud head

In contrast to the upright convection that occurs within the dry slot, the main body of the cloud head itself is characterised by slantwise convection and stratified precipitation. There may also be some upright convection in the form of boundary-layer line convection along the inner edge of the cloud head, and in the form of convective cells at upper levels towards the top of the cloud head (eg Browning and Wang 2001), but the primary circulations in the cloud head are slantwise.

At ana-cold fronts the slantwise circulation is sometimes subdivided to form multiple stacked slantwise convective circulations as discussed by Browning *et al.* (2001). Cloud heads are structured like ana-cold fronts and so it is not surprising that we find similar stacked circulations in cloud heads. Figure 5, adapted from Browning *et al.* (1995 and 1997), portrays the structure of one particularly well observed cloud head. Figure 5(b) shows the banded structure of the cloud top at a stage in its evolution corresponding to that in Fig.2. During the previous 24 hours the cloud head had evolved as shown in Fig.5(a). Seventeen dropsondes were dropped from an aircraft flying along AB between 1623 and 1748 UTC as the tip of the cloud head passed below the flight path. Figure 5(c), depicting the pattern of relative humidity within the vertical section along AB, shows the slantwise orientation of multiple dry and moist layers associated with the stacked slantwise circulations.

The detailed case study of the October 1987 storm presented in the next section will show that the damaging winds occurred in the dry slot close to the tip of a similar multiply banded, hooked cloud head. The cloud head was wrapping around the tail of the bent-back front and air from the tip of the cloud head was entering the region of damaging winds. We shall show that upright and slantwise convection of the kinds described above, together with the associated latent heat effects (evaporation as well as condensation), may have played a role in the local enhancement of the already strong surface winds.

3. THE GREAT OCTOBER 87 STORM REVISITED

(a) Surface analyses

The cyclone of 15/16 October 1987 travelled north-eastwards from west of the Iberian peninsular at 1200 UTC on the 15th to the North Sea close to the England/Scotland border by 1200 UTC on the 16th. The path of the cyclone centre took it across England where the greatest wind damage, to the east of the track, was over south-east England. This is a region with a high density of autographic recording surface weather stations. The availability of a large number of charts from these stations and the detailed cloud and precipitation information provided by Meteosat and weather radar made this an excellent case for examining the mesoscale structure and the possible roles of upright and slantwise convection in increasing the surface winds.

According to Woodroffe (1988), the cyclone reached its lowest central pressure of 952 mb at 0000/16th just north of Brest. This followed a pressure fall of 26 mb over the previous 12 hours, well in excess of the 24 mb in 24 hours that corresponds to explosive development in the terminology of Sanders and Gyakum (1980). Over the same period it went through the life cycle portrayed in Fig.1. By 0000/16th it had just about developed a warm seclusion and the tip of its cloud head was beginning to hook around it as in Fig.2. A good time for a detailed mesoanalysis of the wind fields was centred around 0130/16th as the region of damaging winds began to come inland across southern England. This analysis is given in Section 3(b). To provide a context, we start by showing surface analyses for the two times, 0000 and 0300/16th (Fig.6). The similarity to the structure in the ERICA cyclone of 4-5 January 1989 is noteworthy (see Figs.7(c) and 9(c) of Neiman and Shapiro 1993).

Figures 6(a) and (c) show the surface pressure and frontal analyses at 0000 and 0300 UTC, respectively. They show the formation of the warm seclusion as the bent-back front wraps around the cyclone centre and cold air advances far ahead of it (behind a secondary cold front that corresponds to CF2 in Fig.2). The precise shape of the bent-back front is a little uncertain over the sea but the analysis has been aided by the satellite imagery and

knowledge of how the inner boundary of the cloud head relates to the bent-back front. We show later (Fig.11) that this was the time when the hooked tip of the cloud head was beginning to rotate around the southern flank of the cyclone. The frontal analyses show that the axis of the elongated warm seclusion was also rotating during this period. Pressure gradients are seen to be especially strong around its southern and south-eastern flanks. This and the high speed of propagation of the cyclone (typically 25 ms^{-1}) account for the exceptional rate of pressure rise (23 mb in 3 hours) * after the passage of the cyclone centre at locations such as Netheravon (Fig.7(a)). The later surface wind analyses indicate that the strongest winds were centred at C in Fig.6 (b and d), at the downwind end of the region of tightest pressure gradient.

Figures 6(b) and (d) show the analyses of surface wet-bulb temperature (T_w) at 0000 and 0300 UTC, respectively. The warm seclusion shows up as a 15 deg C bull's-eye at 0000, diminishing to 14 deg C at 0300 UTC as it reaches the south coast of England. A pronounced tongue of cold air can be seen wrapping around the warm seclusion. To the west of the seclusion, T_w drops by 7 deg C within a distance of 20 km or less. A radiosonde released at 0000 UTC from Camborne, 200 km behind the warm seclusion, (not shown) shows that the tongue of cold air was very shallow, being confined there to below 900 mb where there was a 25 m s^{-1} northerly low-level jet (cold conveyor belt). The axis of this tongue of cold air (dashed line) is seen to be within 50 to 80 km of the bent-back front in Fig.6(b) and it passes through the centre of the most damaging winds (C). Indeed it can be assumed that the entire dashed line in Fig.6(b) (and Fig.6(d)) corresponds to an axis of maximum low-level wind speed since this would account for the observed maximum in the advection of low $-T_w$ air. The north-west to south-east distance across the warm core of the encircling low-level wind maximum is 220 km in Fig.6(b), which is almost as small as the 150 to 200-km distance measured in the ERICA cyclone studied by Neiman *et al.* (1993).

* A similar pressure rise of 23 mb in 3 hours was recorded for damaging storm Martin as it propagated across France at 23 m s^{-1} in December 1999; an even faster pressure rise, 29 mb in 3 hours, was recorded for the storm Lothar which propagated across France at 35 m s^{-1} on the previous day (Pearce *et al.* 2001)

Horizontal advection of low-T_w air around the warm core is only part of the story, however, because the rate of advance of the leading edge of this low–T_w air at the surface was exceptionally rapid. The 10 deg C contour, seen arriving at the French coast at 0000 UTC, reached central England by 0300 UTC – a rate of advance of about 47 m s^{-1}. This exceeds the wind strength at the surface, even in gusts, in all places except near C. We attribute this later (section 3(c)) to some air with low wet-bulb potential temperature being brought down to the surface, at least in part by convective downdraughts, from the overrunning flow of dry-intrusion air. Upright convection of sufficient intensity to produce radar-detectable showers was restricted to the leading edge of this flow and this would account for the limited extent of the initial cold (T_w) pool in Fig.6(d). Nevertheless the extent of the cold pool was enough to accelerate the cutting-off of the warm-seclusion air. As recounted by Burt and Mansfield (1988), there is some ambiguity in analysing the surface cold front because the drop in T_w occurred an hour or so before the drop in T. They opted to analyse the T front: in Fig.6 we have analysed the T_w front.

Several of the features in Fig.6(d) show up clearly in autographic traces such as those from Netheravon in Figs.7(b) and (c). Shortly after an exceptional 9 deg C rise in temperature during the passage of the warm front between 2100 and 2300/15th, the relative humidity drops abruptly to below 70% (and the temperature falls more slowly) with the arrival of the secondary cold (T_w) front marked in Fig.6. The dry-bulb temperature then falls by 4 deg C over the period 0000 to 0100/16th and the relative humidity remains fairly low in association with the dry-intrusion air brought down by convective downdraughts. The cold dry conditions prevail until the arrival of warmer and moister air close to the cyclone centre, corresponding to the warm seclusion, the eastern edge of which is seen passing over Netheravon in Fig.7 between 0200 and 0330 UTC. The extent of the dry air is plotted later in Fig.9(b), together with the analysis of peak gusts at 0130 UTC.

(b) Surface gust analysis

Figure 8, from Burt and Mansfield (1988), shows a plot of the highest reported gusts associated with the cyclone. Peak gusts of over 50 m s^{-1} (100 knots) were reported at intervals along a track from Brittany through the Cherbourg peninsula, Sussex and Kent, to the coast of East Anglia. The zone

of strongest wind gusts was centred over the Channel Islands and Cherbourg at 0130 UTC on the 16th; it was close to the Sussex coast at 0330 UTC and was over the Thames estuary at 0430 UTC. The axis of the strongest gusts was about 200 km to the right of the cyclone track, with most of the strong winds occurring within the dry-slot region.

Figure 9(b) shows a detailed mesoanalysis of peak gusts at 0130 UTC. It is based upon autographic wind records from 20 stations in south-east England and the Channel Islands whose locations are indicated in Fig.9(a). The peak gusts from these stations, estimated over 30-minute intervals, have been converted to equivalent measurements in space at 0130 UTC assuming the gust systems to be travelling at 22 m s^{-1} from 217 deg, the velocity of the cyclone centre between 0000 and 0300 UTC . These values are plotted as lines of numbers in Fig.9(a). The underlying assumption in this approach is that the gust systems were translating in a quasi-steady state over a period of typically ± 90 minutes on either side of the 0130 UTC analysis time. In some cases the period of data used from a given station is extended to several hours to carry the measurements over the English Channel but in these cases less reliance can be placed on them. There is also a problem due to local effects and variable instrument exposure which leads to some scatter even for nearby measurements made at roughly the same time. Thus, for example, the underlined values from the Portland RNAS record after 0200 UTC appear to be anomalously high (by about 10 ms^{-1}), perhaps because of over-exposure to winds from west of south. Similarly winds for the Cherbourg area are about 10 m s^{-1} higher as inferred from the Shoreham record compared with those from Jersey, although the spatial trends for both stations are in agreement. This discrepancy may be due in part to Lagrangian time changes but it is probably mainly due to relative over-exposure at Shoreham or, more likely in view of the French measurements in Fig.8, to under-exposure at Jersey.

In addition to an analysis of peak gusts, Fig.9(b) also gives an analysis of surface fronts and the area of low humidity based on data from several thermograph and hygrograph records in southern England. The frontal analysis in Fig.9(b) is consistent with the analyses shown earlier in Figs.6(a) and 6(c) where the warm front, bent-back front and secondary cold front CF2 form one continuous front wrapping around the warm seclusion. Dry air

reached the surface at the position of the analysed cold (T_w) front and the low humidity continued until the arrival of the warm seclusion. The peak-gust analysis in Fig.9(b) draws attention to three main regions of strong winds – A, B and C – associated with the dry air:

Region A: a region containing localised areas (individually labelled A in Fig.9(b)) with gusts up to about 35 m s^{-1}. We shall show that this region was associated with cumulonimbus clouds just ahead of CF2.
Region B: a region with gusts up to about 40 m s^{-1}. We shall show that this region was associated with only shallow non-precipitating cloud.
Region C: a larger zone of even stronger winds, with gusts from 40 to 50 m s^{-1}. We shall show that this region was located in the region of very low or no cloud close to the tip of the hooked cloud head. There is also a sub-region of C, extending behind the bent-back front, under the tip of the cloud head, labelled C'.

Strong-wind Regions A, B, C and C' are identified in the individual anemograph traces from three of the stations in Figs. 10 (a) to (c). Notice the contrasting character of gust regions A and C/C': A is short-lived and peaky whilst C/C' is much more sustained. Information on the strength of the peak gusts from these and three other stations is summarized in Table 1 where the stations are ranked in order of distance to the right (ie south-east) of the cyclone track. All of these stations encountered strong wind gusts associated with Regions A and B except Jersey which was to the right (and perhaps upwind) of the tracks of A and B. The gusts in Regions A and B were in the range 30 to 40 m s^{-1}. However, the very strongest winds were the south-south-westerly winds close to the tip of the hooked cloud head encountered within the core of Region C by stations such as Thorney Island, Jersey (Fig.10(c)) and Shoreham. Stations close to the cyclone track over which the warm seclusion passed, missed the strong winds from Region C. Thus, Portland RNAS (Fig.10(a)) experienced a lull during the passage of the warm seclusion between 0200 and 0300 UTC whilst C travelled by to the south-east. It finally received strong westerly winds from C' once the warm seclusion had passed through.

TABLE 1: PEAK GUSTS (MS^{-1}) IN REGIONS A,B,C AND C' FOR SIX STATIONS LISTED IN ORDER OF DISTANCE (d,KM) TO RIGHT (SOUTH-EAST) OF THE CYCLONE TRACK

	Location	d	Region A	Region B	Region C	Region C'
Portland RNAS	50° 34'N 2° 27'W	24	39	37	-	43
Heathrow Airport	51° 29'N 0° 27'W	67	30	40	-	32
London WC	51° 31'N 0° 7'W	80	31	41	37	-
Thorney Island	50° 47'N 0° 55'W	89	32	34	45	-
Jersey Airport	49° 13'N 2° 12'W	114	-	-	42	-
Shoreham Airport	50° 50'N 0° 17'W	118	35	39	49	-

(c) Cloud systems in the vicinity of the damaging winds

Figure 11(a) shows the infra-red Meteosat image for 0130 UTC corresponding to the gust analysis in Fig.9, and Fig.11(b) identifies some of the key cloud features to be seen in it. A major dry slot extends from Brittany across central-southern England to the Wash and North Sea. To the east of the dry slot is the cold high cloud associated with the polar-front cloud band. To the west is a massive cloud head, with its strongly convex outer edge west of 10°W and the inner boundary of its high cloud situated along the warm front and bent-back front. Banding associated with multiple slantwise convective circulations is seen at the top of the cloud head as described earlier in connection with Fig.5. The cloud-head bands S1, S2 and S3, terminate fairly abruptly close to the coast of Brittany where they begin to hook around the cyclone centre (L). The main region of strong gusts is located close to the leading edge of these cloud-head bands. Farther north-east within the dry slot, Fig.11 shows two other features that we shall also be relating to enhanced surface gusts. One of these is a family of relatively shallow cumulonimbus clouds with their anvils extending north-eastwards ahead of the cold front CF2. The other is a band of shallow cloud labelled CF3 (not reproduced clearly in Fig.11(a)). The feature CF2 corresponds to the main T_w - gradient associated with the secondary cold front identified in Fig.6. The feature CF3 appears to be a shallow convergence line that is scarcely distinguishable in the thermograph and hydrograph traces. We now consider

in more detail the relationship of specific regions of strong wind to the regions of upright and slantwise convection evident in the satellite cloud imagery.

(i) The upright convection associated with Strong-wind Region A.

Comparison of Figs. 9 and 11 shows that the first region (A) of damaging winds was collocated with the upwind end of a row of cumulonimbus clouds within the dry slot. We now examine these cumulonimbus using rainfall data from the Chenies radar (near London) (Fig.12). Figure 12(a) shows the radar display at 0025 UTC when Strong-wind Region A was over parts of central southern England and the Solent. It shows two major areas of rain on either side of the dry slot, one associated with the warm front and the other with the primary cold front (corresponding to CF1 in Fig.2) which was an upper cold front in these parts (hence the open cold-frontal symbols in Fig.12(a) and Fig.6(a)). Within the dry slot itself there is an arc-shaped area of small rain showers. As this area travelled north-north-eastwards the showers became organized as a series of long narrow rainbands orientated almost along the direction of the low-level winds. This is shown in Fig.12(b) which depicts successive positions of the secondary cold front and showers at 0025 and 0140 UTC.

The autographic records at Netheravon (Fig.7(b) and (c)), which apply to the location labelled N in Fig.12(b), show that both the temperature and humidity dropped sharply between 0000 and 0100 UTC during the passage of these showers. Pronounced individual gusts associated with Strong-wind Region A, for example at London Weather Centre (L) in Fig.10(b), can be related to individual rainbands in Figs. 12(b). Presumably some of these gusts were associated with evaporatively cooled downdraughts which would have contributed to the pool of cold surface air analysed in Fig.6(d). This is not the whole story, however, since the wind gusts at some stations reached a peak intensity just after the passage of the convective showers. Thus, although their evaporatively-cooled downdraughts undoubtedly contributed to some of the gusts, they were not the sole cause of the major gusts, even in Region A. Convective showers were even less likely to have been a factor in Strong-wind Regions B and C which were characterised by areas of very shallow cloud and no radar-detectable rain. In these cases a different

combination of mechanisms will have been responsible for enhancing the strength of the surface winds. A possible clue to these mechanisms is to be found in the proximity of the tip of the cloud-head to Strong-wind Region C which we consider next.

(ii) The relationship of slantwise convection to Strong-wind Region C

The dashed lines in Fig.11(b) draw attention to the banded cloud tops within the cloud head. Marked banding was also evident in the low-level rainfall distribution as seen in the radar-network imagery (not shown) where the bandedness extended along both the bent-back front and the warm front. Band spacing was 40 to 70 km in the low-level radar imagery, increasing to up to about 100 km at cloud-top level in the satellite imagery. By analogy with the detailed case study summarized in Fig.5, we propose that the bands are a manifestation of multiple stacked slantwise convective circulations. These are transverse circulations that are superimposed upon the strong flows around the cyclone centre along the axes of the cloud-head bands. Over the 5-hour period from 2030/15th up to 0130/16th, the ends of the cloud bands were propagating even more slowly than the cyclone centre, at only 16 m s^{-1} (although this increased to 27 m s^{-1} during the 4 hour period after 0130 UTC). With surface gusts generally exceeding 30 m s^{-1}, the low-level air in these regions would have been travelling faster than the rate of propagation of the ends of the cloud bands. Therefore, relative to the cloud bands, the air within the bands will have been advecting, eastwards and then north-eastwards, into the region just ahead of them. The magnitude of this (relative) advection speed is an indirect measure of the rate of evaporation of the cloud material.

Figure 11(b) shows that the ends of these bands, where they terminate in the dry slot, are only about 100 km away from Jersey (J). Peak gusts at Jersey at this time were 40 m s^{-1}. Indeed there was a consistently close relationship between the location of the strongest gusts and the ends of the cloud-head bands as the system travelled from the English Channel into and across southern England. Successive positions of the tips of the cloud-head bands are plotted in Fig.13 alongside the axis (AB) of strongest surface gusts taken from Fig.8. Along this axis, Jersey experienced the 40 m s^{-1} gusts from 0100 to 0230 UTC/16th and Shoreham (S) experienced even stronger gusts of

about 50 m s^{-1} from 0300 to 0400 UTC when the tips of the cloud-head bands were again 100 km to the west. This consistent relationship is evidence linking the strongest surface winds to cloud-head air exposed to rapid evaporation and presumably, therefore, to strong descent and/or mixing with very dry air.

Figure 14 is a schematic plan-view visualization of the stacked slantwise circulations associated with the cloud-head bands, S1, S2 and S3, in Fig.11. The three hatched arrows labelled SU1, SU2 and SU3 are the ascending limbs of the slantwise circulations. The three stippled arrows, labelled SD1, SD2 and SD3, are the corresponding descending limbs undercutting the shaded arrows as they circulate around the flank of the cyclone. The hatched arrows are shown terminating south of the cyclone centre (L) where the cloud tops suddenly lower, indicating the termination of ascent and evaporation of cloud. Of course this flow continues on, but as a cloudless flow (except where it gets around to the north-east of the cyclone centre when renewed ascent leads to reformation of the stratiform cloud bands especially at later times – not discussed further in this paper). The three descending flows meanwhile approach the boundary layer and produce strong wind gusts at the surface at and behind the convergence lines labelled A, B and C (perhaps related to Strong-wind Regions A, B and C, respectively).

(d) *Hypotheses relating to the role of slantwise convection and evaporation*

Shutts (1990) found, on the basis of modelling studies of the October 87 Storm, that two thirds of the central-pressure deepening could be ascribed to latent-heat release. This occurs due to condensation in the slantwise ascent mainly in the cloud head. As also indicated by the model results of Grønås (1995), this can play a dominant role in generating the damaging winds that occur near the tip of the cloud head. But the fact that the most severe winds occurred close to and just downwind of the evaporating cloud-head tip is strongly suggestive of a role also for the evaporative heat sinks in this region. We hypothesize the following mechanisms whereby the evaporation associated with slantwise convection might enhance the strength of the surface winds:

- Slantwise circulations in the cloud head lead to evaporative cooling in the descending parts. This cooling is especially strong just to the south of the cyclone where the tip of the cloud head begins to hook around. Here very dry air from the dry intrusion can enter the descending limb of the slantwise circulation at quite a low level.
- The evaporative cooling produces a hydrostatic increase in the surface pressure beneath it within the tip of the cloud hook south of the cyclone centre. This (and the rapid cyclone movement) accounts for the exceptionally rapid rise of surface pressure after the passage of the cyclone centre. The associated large horizontal pressure gradient acts geostrophically to increase the windspeed in this region.
- The evaporative cooling acts to intensify the transverse slantwise circulation on the mesoscale. This increases the downward transport of the high-momentum air in the descending branch. Evaporative cooling is most effective where there is sublimation of ice, as shown in the high-resolution modelling study of FASTEX cyclones by Forbes and Clark (2002). However, in the present case we suspect it is the evaporation of cloud water below the zero-degree level that is most important in generating descent close to the surface.
- The existence of not just one broadscale transverse circulation but rather a series of stacked shallow transverse circulations, increases the amount of evaporation and spreads it over a larger region because it produces more sheared interfaces with Richardson-Number-controlled mixing across them as described in Browning (1995). This may lead to a significant heat sink even at the low levels where water rather than ice is evaporating
- The resulting low-level jets of evaporatively cooled low $-\theta_w$ air, SD1, SD2 and SD3 in Fig.14, emanating from the hooked end of the cloud head, descend close to the ground behind features identified in Fig.14 as A, B and C. Feature A may be identified with the secondary cold front (CF2) where convective showers with downdraughts give relatively isolated areas of strong surface gusts and contribute to a mesoscale pool of low- θ_w air at the surface. The earlier evaporative cooling of air leaving the tip of the cloud head may have reduced the static stability and contributed to the generation of the upright

convection in this region. Feature B may perhaps be identified with the convergence line seen by satellite as a shallow cloud band, and which was also associated with strong surface gusts. Feature C, closest to the tip of the cloud head, marks the leading edge of a 250-km wide region containing the strongest winds of all, where the slantwise descent brings down air that evidently gives rise to gusts at the surface as a result of intense boundary-layer turbulence associated with low static stability but in the absence of deep convection.

In summary, all the regions of damaging wind described above occur close to or just in advance of the tip of the hooked, and multiply-banded, cloud head associated with slantwise circulations. The cloud head is characterised by a low-level jet (cloud-head jet) associated with Strong-wind region C' and this intensifies downwind of the tip of the cloud head (Strong-wind regions A, B and C). Adopting a similar terminology to Grønås (1995), we refer to these regions collectively as 'the sting at the end of the tail' where the tail is the bent-back front associated with the cloud head. Air leaving the tip of the cloud head experiences strong evaporative cooling and the likely role of evaporation (in addition to the well-known effect of condensation) in increasing the strength of the surface winds is our principal message.

We have presented evidence of the importance of the slantwise convective circulations in the hooked cloud head but have not addressed the question of the dynamical cause of these circulations. It is tempting, in view of the banded nature of the cloud head, to attribute these circulations to conditional symmetric instability (CSI). This is particularly compelling in view of the small scale of the circulations which are believed to resemble the stacked slantwise convective circulations documented by Browning *et al.* (2001). However, Schultz and Schumacher (1999) draw attention to the dangers of jumping to conclusions in the absence of additional evidence. Further evidence for CSI in cloud heads has been obtained by Dixon *et al.* (2002), and Shutts (1990) has provided such evidence specifically for the October 87 Storm. Shutts estimated values of slantwise convective available potential energy (SCAPE) in excess of 1000 J kg^{-1} in the warm air of the October 87 Storm. Unfortunately the evidence for CSI is somewhat

weakened by the 2-dimensional assumption underlying the calculation of SCAPE. Nevertheless Shutts argues that the small scale and intensity of the explosively developing October 87 Storm is a direct result of vortex spin-up due to slantwise convective mass transfer. Reed and Albright (1986) make a similar suggestion in their study of an extreme cylogenesis event in the eastern Pacific, and Kuo and Reed (1988) support this idea by carrying out a diagnostic analysis of a numerical simulation of the same event. Forbes and Clark (2002) point out that the heating/cooling dipole, due to condensation/evaporation in the ascending/descending limbs of the slantwise circulations, generates slantwise potential vorticity sheets which may locally enhance the moist symmetric instability and the strength of the slantwise circulations.

4. TWO OTHER STORMS WITH DAMAGING WINDS

Missing from the above study are observations of winds aloft near the tip of the cloud head. We therefore supplement this study with partial results from two other extratropical cyclones. Neither was as severe as the Great October Storm but both gave damaging winds near the tip of the cloud head.

(a) The cyclone of 26 February 2002

Figures 15(a) and 16(a) are radar-network and satellite pictures showing the patterns of precipitation and cloud associated with a small cyclone as the tip of its hooked cloud head approached the west coast of Wales at 0300 UTC on 26 February 2002. This cyclone produced minor wind damage. Some of it was associated with bands of convective line elements (one band can be seen extending from Brest to Birmingham and another from Cardiff to Chester), and some was associated with the tip of the cloud-head hook. A 42 m s^{-1} gust was reported at Macclesfield in the path of the cloud-head hook. The reason for choosing to present this case is that the tip of the cloud head passed directly over the MST (Mesosphere-Stratosphere-Troposphere) radar at Aberystwyth, which provided useful measurements of the atmospheric structure aloft.

Time-height records of windspeed and returned power from the Aberystwyth radar are shown in Figs.17(a) and (b), respectively. They are for the period 0000 to 0800 UTC, a few hours on either side of the time of Figs.15(a) and 16(a). Figure 17(a) shows a low-level jet below 4km, with a maximum speed of 45 m s^{-1} at 2.2km at 0320 UTC, corresponding to the passage of the tip of the cloud head. This is labelled the cloud-head jet (CHJ). Figure 17(b) shows regions of high received power (white and pale grey) at low levels corresponding to the main interface between moist low-level air and very dry air in the dry intrusion. This interface descends down from 5 km to about 3 km in places between 0130 and 0230 UTC during the passage of the dry slot. This, together with the very low returned power just above the lowered interface, is indicative of an intrusion of dry, possibly stratospheric, air and indeed the entire signature of returned power in Fig.17(b) is similar to that encountered in a suspected stratospheric intrusion ahead of a cloud head documented by Browning and Dicks (2001).

We have shown that the cloud head and its associated jet (Fig.17(a)) are situated beneath the dry intrusion (Fig.17(b)). Between 0300 and 0400 UTC in Fig.17(b) there are several sloping layers of maximum returned power within the cloud head which can be interpreted in terms of sloping stable layers (Ottersten 1969). The positions of these layers are sketched as thin black lines superimposed on the windspeed display in Fig.17(a) to show that the cloud-head jet occurs in association with these stacked stable layers. Although it does not show up very clearly in Fig. 17(a) there is some evidence of laminations in wind speed due to slantwise circulations in these layers. As for the Great Storm of October 87, this is the very region where evaporation can be expected to have been effective in intensifying the local circulations. Figure 16(a) shows that the tip of the cloud head is quite wide, consistent with the presence of the multiple circulations; however, the radar picture in Fig. 15(a) shows that, probably as a result of the evaporation, only a single rather narrow band of rain reaches the surface in this region. Evidence of multiple bandedness in the cloud-head structure is weak in Fig.16(a) but it is much clearer in the case considered next.

(b) The cyclone of 30 October 2000

The main thrust of this paper has been to use purely observational data to establish the nature of the mesoscale and convective processes in the strong-wind regions. However, our final piece of analysis exploits the output from an operational run of the mesoscale version of the Met Office Unified Model, hereafter referred to simply as the mesoscale model. (No high-resolution operational model runs were available for the 1987 storm so long after the event). We shall show that the operational mesoscale model, although not able to resolve the multiplicity of slantwise circulations, is capable of resolving some other key aspects of the structures described earlier in this paper, thereby motivating the further modelling studies that are being pursued in a second phase of this research.

The cyclone of 30 October 2000 deepened explosively by 60 mb in 24 hours as it travelled east-north-eastwards towards and across the British Isles. It finally attained an estimated depth of 941 mb in the North Sea where it produced sustained winds in excess of hurricane force. The strongest winds began to develop just to the south of the cyclone centre as it crossed the east coast of England. A surface gust of 41 m s^{-1} was recorded at Grimsby near the hooked tip of the cloud head between 0900 and 1000 UTC roughly corresponding to the time of the radar image in Fig.15(b).

The mesoscale model output in Fig.18 shows the mature cyclone shortly afterwards, at 1200 UTC, when it was centred in the North Sea (Fig. 18(a)). The model-derived pattern of relative humidity at 500 mb (Fig.18(b)) closely resembles the 1200 UTC satellite image in Fig.16(b) in that it depicts the cloud head with its tip hooked around the southern edge of the cyclone centre. The distribution of 900-mb vorticity in Fig.18(c) draws attention to the strongly sheared frontal zone associated with the bent-back front culminating in the cloud-head hook; it also shows that the cyclone is at Stage IV of the frontal-fracture process shown in Fig.1, with a break in the vorticity strip associated with the main cold front ahead of the cyclone centre where it intersects the warm-frontal vorticity strip. The patterns of θ_w and relative humidity at 900 and 800 mb, respectively, (Figs.18(e) and (d)) show moist, low -θ_w air curving around the cyclone centre in the region of the hooked tip of

the cloud head. Figure 18(f) shows that there is a well defined mesoscale low-level jet (ie a cloud-head jet) in this region, with peak winds of 45 to 50 m s^{-1}. It is significant that this cloud-head jet is distinct from another low-level jet which is associated with the better understood warm-conveyor-belt flow of high-θ_w air just ahead of the main cold front.

Vertical cross sections south-north through the cloud-head jet are shown in Figs.19(a) and (b). The cloud-head jet, labelled CHJ at 54½°N in Fig. 19(a), is quite distinct from the warm-conveyor-belt low-level jet at 49°N which is linked to the upper-level polar-front jet J. The relative-humidity pattern in Fig.19(b) shows deep regions of near-saturated air corresponding to both the polar-front cloud band and the cloud head. These are separated by dry-intrusion (partly stratospheric) air coming down to quite low levels. The cloud head extends southwards on the western side of this section and its tip reappears in Fig.19(b) as a much shallower feature penetrating into the dry-intrusion air at levels mainly below 700 mb. Figure 19(a) shows that this shallow cloud-head feature is closely related to the compact but intense cloud-head jet. This CHJ is part of the strong flow – the sting at the end of the tail – that was interpreted in section 3 as being strongly influenced by evaporative cooling. The maximum model-derived wind speed in the CHJ of 55 m s^{-1} is not far short of the 850-mb maximum of 60 m s^{-1} inferred by Grønås (1995) in his modelling study of Norway's worst storm of the 21st century. A θ_w cross section corresponding to Fig.19 (not shown) reveals that the CHJ coincides with the minimum value of θ_w, ie the cold conveyor belt, near the southern boundary of the warm seclusion. It also shows that, as in the Grønås study, and in other observational studies (eg. Fig.14 of Shapiro *et al.* 1999), the θ_w contours in the lower troposphere were fairly close to the vertical in this region. Since the air was near saturation in parts of this region, this indicates weak stability with respect to both upright and slantwise convective instability. It is interesting that in practice the atmosphere at the tip of the cloud head appears to release instability mostly via slantwise convection.

5. CONCLUSIONS

A detailed analysis has been presented of the observed mesoscale structure associated with the damaging winds in the Great Storm in south-east England in October 1987. The study has been supported by brief analyses of two other (less) damaging extratropical cyclones in the UK. These studies have focussed in each case on regions of strong winds close to the cyclone centre which are in a region of the dry slot that is distinct from the well-known belt of strong low-level winds that accompanies the warm conveyor belt along the primary cold front. We refer to this dry-slot wind maximum as the sting at the end of the tail, terminology similar to that used by Grønås (1995). A low-level jet (or cloud-head jet) occurs within the tip of the cloud head when the bent-back front and associated cloud head begin to hook around towards the right flank of the cyclone into the dry-intrusion air that characterises the dry-slot. Surface winds associated with this low-level jet become even stronger as the air exits at the tip of the cloud head and enters the dry slot. The dry-slot wind maximum does not occur in all cyclones; rather, it is believed to be associated only with cyclones that go through the four stages of Shapiro and Keysers' (1990) frontal-fracture process. The most damaging storms in this category generally undergo a period of explosive development and are distinguishable in satellite imagery not only by a pronounced cloud head (Böttger *et al.* 1975) but by a cloud head that has a distinctly hooked tip.

Shutts (1990), in an earlier modelling study of the October 87 Storm, developed the hypothesis "that the cloud head, known to accompany explosive developments which produce hurricane-like cores, is a manifestation of intense slantwise convective ascent triggered by the approach of an upper-level trough". He found that the associated release of latent heat accounted for two-thirds of the deepening. In the present paper we have focussed on the additional role of evaporative heat sinks in the cloud-head region. The damaging dry-slot wind maximum has been shown to be situated immediately downwind of a region of rapid evaporation where cloud and precipitation dissipate entirely as the air exits from the tip of the cloud head. This is essentially where cloudy cold-conveyor-belt air blends with the dry-intrusion air. We propose several hypotheses which together might

account for how the evaporation increases the already strong surface winds in this region:

(1) The evaporative cooling is presumed to lead to a positive hydrostatic pressure anomaly which may account for the locally increased pressure gradient and geostrophic wind at low levels on the right rear flank of the cyclone.

(2) The evaporative cooling leads to enhanced transverse circulations within slantwise convection that characterises the cloud head, and the descending limb of the circulation transports high-momentum air towards the surface. As explained by Forbes and Clark (2002), the heating/cooling dipole, due to condensation/evaporation in the ascending/descending limbs of slantwise circulations, generates a slantwise potential vorticity sheet. This locally enhances the moist symmetric instability and the strength of the slantwise circulation.

(3) The slantwise convection in the cloud head tends to be broken up into multiple coexisting layers of ascending and descending flows. These resemble the stacked slantwise convective circulations identified by Browning *et al.* (2001) which, because of the small scale of the circulations, were attributed to conditional symmetric instability. This multiplicity of slantwise circulations increases the number of interfaces for mixing the cloudy cold-conveyor-belt flow with the very dry dry-intrusion flow, and it leads to more efficient evaporation. It also spreads out the evaporative effects laterally, thereby helping to increase the lateral extent of the region of damaging surface winds.

(4) The evaporative cooling, especially if the evaporation is completed before any precipitation reaches the surface, acts to reduce the static stability and hence Richardson Number, thereby promoting more mixing of high-momentum down through the boundary layer even though deep convection may be inhibited

(5) As the evaporatively cooled air exiting from the cloud head advances farther ahead of the tip of the cloud head, it begins to overrun progressively warmer boundary-layer air (W2 air in the conveyor-belt parlance) in the dry-slot. This may lead to some upright convection. The resulting convective showers produce their own local downdraughts which give rise to further surface gusts of a more localised nature.

This observational study has been stimulated by the availability of a dense array of surface observations and informative geostationary imagery in the strong-wind region of the Great October Storm. Even so, the ideas presented here have had to be based upon inferences, some of them inspired by other case studies, as for example the inference that the banded structure of the cloud-head tip in the October Storm was similar to that in the FRONTS-92 cyclone (Browning *et al.*1995 and 1977) in which dropsondes were used to reveal the existence of multiple slantwise circulations. Thus these ideas have been presented as a series of hypotheses which require validation and quantification by means of high-resolution modelling studies. Such studies have been initiated by P. Clark, (Joint Centre for Mesoscale Meteorology) and will be reported in Part II. These modelling studies are presently concentrating on the Great October Storm because of the quality of the observational data for validation. Unfortunately, despite the large impact this event had on the Meteorological Office at the time, none of the high-resolution (Fine Mesh) operational model runs performed at the time of the Great Storm (Gadd and Morris 1988) nor the subsequent improved model rerun (Shutts 1990) has been archived. Consequently the new modelling studies make use of fresh model runs with the New Dynamics version of the Met Office Unified Model initialised from ECMWF Re-Analysis (ERA) data. It is hoped that this line of research will lead to better representation of convective and mesoscale processes within operational models and contribute to improved prediction of a class of storm that inflicts a huge amount of damage in Europe.

ACKNOWLEDGEMENTS

The writer is grateful to Mike Bader for making available original autographic records, imagery, working diagrams and charts from earlier studies conducted within the Met Office by himself, Geoff Monks and Martin Young. Thanks are due to Kirsty Lewis and Gareth Roberts, Univ. of Reading, for contributing to the analysis in Section 4(b), to Chang-Gui Wang for help with the production of the computer-generated diagrams and to Dick Reed, Cliff Mass and Dave Schultz for their help in tracking down the origin of the term "poisonous tail of the bent-back (front)". The data from the MST radar, Meteosat and ERA, were provided by the British Atmospheric Data Centre,

EUMETSAT and ECMWF, respectively. The Joint Centre for Mesoscale Meteorology is supported by the Met Office and the Department of Meteorology, University of Reading, and by the Natural Environment Research Council through its support of the Universities Weather Research Network (UWERN).

REFERENCES

Bader, M.J., Forbes, G.S., Grant, J.R., Lilley, R.B.E. and Waters, A.J. 1995 *Images in weather forecasting.* Cambridge University Press

Blier, W. and Wakimoto, R.M. 1995 Observations of the early evolution of an explosive oceanic cyclone during ERICA IOP 5. Part I : synoptic overview and mesoscale frontal structure. *Mon.Weather Rev.,* **123,** 1288-1310

Böttger, H., Eckardt, M. and Katergiannakis, U. 1975 Forecasting extratropical storms with hurricane intensity using satellite information. *J.Appl.Meteorol., **14**, 1259-1265*

Browning, K.A. 1995 On the nature of the mesoscale circulations at a kata-cold front. *Tellus*, **47A,** 911-919

Browning K.A. 1999 'Mesoscale aspects of extratropical cyclones: an observational perspective'. Pp.265-283 in *The life cycles of extratropical cyclones.* Eds: M.A.Shapiro and S. Grønås. American Meteorological Society, Boston, Mass, USA

Browning, K.A. 2003 'Mesoscale substructure of extropical cyclones observed by radar'. Pp.xxx-xxx. In *The Dave Atlas Symposium Monograph.* Eds. R.M. Wakimoto and R. Srivastava, American Meteorological Society. Boston, Mass., USA. In press

Browning, K.A. and Dicks, E.M. 2001 Mesoscale structure of a polar low with strong upper-level forcing. *Q.J.R Meteorol.*, **127**, 359-375

Browning, K.A., and Monk, G.A. 1982 A simple model for the synoptic analysis of cold fronts. *Q.J.R.Meteorol.Soc.*, **108**, 435-452

Browning, K.A. and Roberts, N.M. 1999 Mesoscale analysis of arc rainbands in a dry slot. *Q.J.R Meteorol.Soc.*, **125,** 3495-3511

Browning, K.A., and Wang, C.-G. 2002 Cloud-top striations above ana-cold frontal circulations. *Q.J.R.Meteorol.Soc.*, **128,** 477-499

Browning, K.A., Clough, S.A., Davitt, C.S.A., Roberts, N.M., Hewson, T.D. and Healey,P.G.W. 1995 Observations of the mesoscale sub-structure in the cold air of a developing .frontal cyclone. *Q.J.R.Meteorol.Soc.*, **121**,1229-1254

Browning, K.A., Roberts, N.M. and Sim, C.S. 1996 A mesoscale vortex diagnosed from combined satellite and model data. *Meteorol.Apps.*, **3**, 1-4

Browning, K.A., Ballard, S.P. and Davitt, C.S.A. 1997 High-resolution analysis of frontal fracture. *Mon.Weathe Rev.*, **125**, 1212-1230

Browning, K.A., D. Chapman, D. and Dixon, R.S. 2001 Stacked slantwise convective circulations. *Q.J.R.Meteorol.Soc.*, **127,** 2513-2536

Burt, S.D. and Mansfield, D.A. 1988 The Great Storm of 15-16 October 1987. *Weather,* **43**, 90-114

Carr, F.H. and Millard, J.P. 1985 A composite study of comma clouds and their association with severe weather over the Great Plains. *Mon.Weather Rev.,***113**, 370-387

Dixon R.S., Browning, K.A. and Shutts, G.J. 2002 The relation of moist symmetric instability and upper-level potential-vorticity anomalies to the observed evolution of cloud heads. *Q.J.R.Meteorol.Soc.,* **128,** 839-859

Forbes, R.M. and Clark, P.A. 2002 Sensitivity of extra-tropical cyclone mesoscale structure to the parametrization of ice microphysical processes. *Q.J.R.Meteorol.Soc.*, **128**, xxx – xxx In press.

Gadd, A.J. and Morris, R.M. 1988 Guidance available at Bracknell for the storm of 15/16 October 1987, and the forecasters' conclusions at the time. *Meteorol.Mag.*, **117**, 110-117

Griffiths, M., Thorpe, A.J. and Browning, K.A. 2000 Convective destabilisation by a tropopause fold diagnosed using potential-vorticity inversion. *Q.J.R.Meteorol.Soc.*, **126**, 125-144

Grønås, S. 1995 The seclusion intensification of the New Year's day storm 1992. *Tellus,* **47A**, 733-746

Kuo, Y.-H. and Reed, R.J. 1988 Numerical simulation of an explosive deepening cyclone in the eastern Pacific. *Mon.Weather Rev.,* **116**, 2081-2105

McCallum, E. 1990 The Burns' Day Storm, 25 January 1990. *Weather,* **45**, 166-173

Neiman, P.J. and Shapiro, M.A. 1993 The life cycle of an extratropical marine cyclone. Part I: Frontal-cyclone evolution and thermodynamic air-sea interaction. *Mon.Weather Rev.,* **121**, 2153-2176

Neiman, P.J. and Shapiro, M.A., Donall, E.G. and Kreitzberg, C.W. 1990 Diabatic modifications of an extratropical marine cyclone warm sector by cold underlying water. *Mon.Weather Rev.,* **118**, 1576-1590

Neiman, P.J. and Shapiro, M.A. and Fedor, L.F. 1993 The life cycle of an extratropical marine cyclone. Part II: Mesoscale structure and diagnostics. *Mon.Weather Rev.,* **121**, 2177-2199

Newton, C.W. and Holopainen, E.O. (Eds.) 1990 *Extratropical cyclones : the Eric Palmén memorial volume.* American Meteorological Society, Boston, Mass., USA

Ottersten, H. 1969 Mean vertical gradient of potential refractive index in turbulent mixing and radar detection of CAT. *Radio Science*, **4,** 1247-1249

Pearce, R., Lloyd, D. and McConnell, D. 2001 The post-Christmas 'French' storms of 1999. *Weather*, **56**, 81-91

Pedgley, D.E. 1997 The Fastnet storm of 1979: a mesoscale surface jet. *Weather*, **52**, 230-242

Reed, R.J. and Albright, M.D. 1986 A case study of explosive cyclogenesis in the eastern Pacific. *Mon.Weather Rev.,* **114**, 2297-2319

Sanders, F. and Gyakum, J.R. 1980 Synoptic-dynamic climatology of the "bomb". *Mon.Weather Rev.,* **108**, 1589-1606

Schultz, D.M. and Schumacher, P.N. 1999 The use and misuse of conditional symmetric instability. *Mon.Weather Rev.,* **127**, 2709-2732;corrigendum, **128**, 4143-4148

Shapiro, M.A. and Grønås, S. (Eds.) 1999 *The life cycles of extratropical cyclones.* American Meteorological Society, Boston, Mass, USA

Shapiro, M.A. and Keyser, D. 1990 'Fronts, jet streams and the tropopause'. Pp.167-191 in *Extratropical cyclone: the Eric Palmén memorial volume.* American Meteorological Society, Boston, Mass., USA

Shapiro, M., Wernli, H., Bao, J.-W., Methven, J., Zou, X., Doyle, J., Holt, T., Donall-Grell, E. and Neiman, P. 1999 A planetary-scale to mesoscale perspective of the life cycles of extratropical cyclones : the bridge between theory and observations. Pp.139-185 in *The life cycles of*

extratropical cyclones. American Meteorological Society, Boston, Mass, USA

Shutts, G.J. 1990 Dynamical aspects of the October Storm, 1987 : a study of a successful fine-mesh simulation. *Q.J.R.Meteorol.Soc.,* **116,** 1315-1347

Ulbrich, U., Fink, A.H., Klawa, M. and Pinto, J.G. 2001 Three extreme storms over Europe in December 1999. *Weather, **56**, 70-80*

Wakimoto, R.M., Nolan, N.T. and Liu, C. 1995 Observations of the early evolution of an explosive oceanic cyclone during ERICA IOP 5. Part II: airborne Doppler analysis of the mesoscale circulation and frontal structure. *Mon.Weather Rev.,* **123**, 1311-1327

Woodroffe, A. 1988 Summary of weather pattern developments of the storm of 15/16 October 1987. *Meteorol.Mag,* **117**, 99-103

Young, M.V.and Grahame, N.S. 1999 Forecasting the Christmas Eve storm 1997. *Weather*, **54**, 382-391

FIGURE LEGENDS

Fig. 1 Conceptual model of the life cycle of an extratropical cyclone: (I) incipient frontal cyclone; (II) frontal fracture; (III) bent-back front and frontal T-bone; (IV) warm-core frontal seclusion. Upper diagram : sea-level pressure, solid lines; fronts, bold lines; cloud signature, shaded. Lower diagram : temperature, solid lines; cold and warm air currents, solid and dashed arrows, respectively. (From Shapiro and Keyser 1990).

Fig.2 Conceptual model of the principal airflows in an extratropical cyclone undergoing transition from Stage III to Stage IV in Fig.1. The flows are drawn relative to the cyclone system which is travelling towards the top right-hand corner of the page. The two main cloud features are shaded: (i) the polar-front cloud band, which is associated with the ascent of the primary warm conveyor belt (broad arrow labelled W1) as it travels parallel to the primary cold front (CF1), and (ii) the cloud head (to the left of the bent-back front WF2), which is associated with the ascent of the secondary warm conveyor belt (W2) and the cold conveyor belt (bold dashed line representing a flow beneath W1 and W2). Notice the hooked end of the cloud head where the cold conveyor belt intrudes into the dry slot behind the secondary cold front (CF2) beneath an intrusion of recently-descended very dry air (thin dashed line). (From Bader *et al.* 1995).

Fig.3 Idealised evolution of the hooked tip (H) of a cloud head (E) in a rapidly developing extratropical cyclone (centred at x) The cyclone reaches its maximum development at stage (b). (From Bader *et al.* 1995).

Fig.4 Three-hourly sequence of mesoscale-model diagnostics showing the effect of a vortex on the evolving three-dimensional structure of a wet-bulb potential temperature surface defining the middle part of a frontal zone. Contours show the surface at 900 mb (thin line), 700 mb (thick line) and 500 mb (dashed line): there is potential instability where the thick line advances ahead of the thin line. The almost

circular contour, with shading, shows the vortex centre at 700 mb (absolute vorticity about 2 x $10^{-4}s^{-1}$). (From Browning *et al.* 1996).

Fig.5 Evidence of multiple slantwise circulations within a developing cloud head observed in the FRONTS-92 experiment.

(a) Plan outlines of cloud head (<-15 deg C) at 12-hour intervals. The long arrow shows track of cyclone centre (L). AB shows location of section in (c).

(b) Plan view of cloud head in more detail, at the latest time in (a), showing the multiply banded cloud tops (thickly stippled shading ≤ - 30 deg C, thinly stippled shading ≤ -20 deg C, outer wavy line –15 deg C).

(c) Vertical section along AB in (a), derived from 17 dropsondes (arrows at top of diagram), showing sloping layers of moist and dry air associated with the multiple circulations (shading represents RH > 80%).

(Simplified from Browning *et al.* 1995 and 1997).

Fig.6 Mesoanalyses of the intense cyclone on 16 October 1987; (a) and (b) are for 0000 UTC; (c) and (d) are for 0300 UTC. Mean-sea-level pressure (isobars every 4 mb) and frontal analyses are shown in (a) and (c). Surface wet-bulb temperature (isolines every 1 deg C) are shown in (b) and (d). The long dashed arrow shows the axis of the cold flow which (relative to the system) is beginning to encircle the warm seclusion: the strongest surface winds were situated along this axis, at C (cf. detailed gust analysis in Fig.9). The open cold-frontal symbols in (a) represent the northern part of the primary cold front where it is mainly an upper-level feature. The other cold front is the main secondary cold front which is linked to the warm front via a bent-back front encircling the warm seclusion.

Fig.7 (a) Pressure (mb, unadjusted), (b) temperature (°C) and (c) relative humidity (%) traces for the period 1000 UTC, 15 October to 1200 UTC, 16 October 1987, at Netheravon (51° 14'N 01°47'W). Warm front (WF), warm seclusion (WS) and dry slot (DS) are labelled.

Fig.8 Highest reported gusts (knots), with contours every 10 knots, over southern England, Wales and the near continent, 16 October 1987. The data were obtained mostly from anemograph data; those in parentheses are unchecked synoptic messages, or estimated values over France. (From Burt and Mansfield 1988).

Fig.9 (a) Raw data and (b) mesoanalysis of the distribution of peak surface wind gusts (m s^{-1}) at 0130 UTC, 16 October 1987, derived from anemograph traces at 20 stations*. Station locations are indicated by the circles in (a) and half-hourly peak-gust measurements for each station have been converted to a series of measurements at equivalent spatial locations based on the system velocity at this time of 22 m s^{-1} from 217 deg. Isotachs in (b) are at 5 m s^{-1} intervals. Some of the fine structure in (b) is based on observations extracted at finer temporal resolution than plotted in (a). Isotachs shown dashed deviate from the data in (a) to take into account French data in Fig.8. The anomalously high underlined values at one of the Stations (Portland RNAS) are discussed in the text. Four regions of strong winds, referred to in the text, are labelled A,B,C and C'. The thick line in (b) represents the warm and bent-back front and the secondary cold front CF2 as derived from thermograph records. The thick dashed line in (b) shows the extent of dry air (RH<80%) as derived from hygrograph records.

*(Footnote to Fig.9: The 20 stations used in Fig. 9, from left to right, are Cardiff (Rhoose), Plymouth (Mount Batten), Bristol Weather Centre, Exeter Airport, Yeovilton, Brize Norton, Netheravon, Portland RNAS, Middle Wallop, Bournemouth Hurn Airport, Southampton Weather Centre, London Heathrow, London Weather Centre, Guernsey, Thorney Island, Jersey, Shoreham, Shoeburyness, Herstmonceux and Manston).

Fig.10 Raw anemograph traces (top, direction in deg.; bottom, speed in knots) for (a) Portland RNAS, (b) London Weather Centre and (c) Jersey (locations given in Table 1). Times of gusts associated with Strong-wind regions A,B,C and C' are labelled.

Fig.11 (a): Meteosat infra-red image for 0130 UTC, 16 October 1987, and (b): key to features in (a), showing the polar-front cloud band extending from France to the North Sea and a large cloud head over and to the south-west of the British Isles, with cloud-top bands (S1, S2 and S3) terminating near the tip of the cloud head. The position of the cyclone centre (L) and parts of the surface fronts are marked: using the labelling convention in Fig.2, CF2 corresponds to the dominant surface cold front plotted in Fig.6, and CF3 corresponds to a shallow convergence line behind CF2. Cumulonimbus clouds ahead of CF2 are shown stippled. J marks the location of Jersey which was experiencing gusts to 40 m s^{-1} at this time.

Fig.12 Rainfall patterns observed at 5-km resolution out to 210 km by the Chenies radar on 16 October 1987, with fronts superimposed. (a): complete rainfall pattern at 0025 UTC. (b): parts of rainfall patterns at 0025 and 0140 UTC for the rain showers associated with the secondary cold front (CF2) only. The locations of Netheravon (N), Heathrow Airport (H) and London Weather Centre (L) are shown in (b).

Fig.13 Successive positions of the ends of the dominant cloud-head bands at 2030, 2300, 0130, 0400 and 0530 UTC 15/16 October 1987, plotted alongside the axis (AB) of strongest surface gusts obtained from Fig.8. J and S mark the positions of Jersey and Shoreham. Times of strongest gusts at J and S are given in the text.

Fig.14 Conceptual model depicting stacked slantwise convective circulations wrapping around the bent-back front of an intense extratropical cyclone. The cyclone is shown at the stage of minimum central pressure when the bent-back front (thick line) has almost encircled warm air near the cyclone centre (L). Three slantwise convective circulations are sketched, each consisting of a slantwise ascending, SU (hatched), and a slantwise descending, SD (stippled), branch. Each (SU+SD)-pair can be interpreted as a transverse circulation (radially outward from the cyclone centre) superimposed on a strong

flow along the axis of the arrows approximately parallel to the bent-back front. The SU parts of these circulations are cloudy with precipitation, and they are collectively responsible for the hooked tip of the cloud head. The evaporatively cooled SD parts of the circulations descend into the boundary layer behind a series of secondary cold fronts or convergence lines (A, B and C) and they are responsible for the very strong surface wind gusts that occur near and just ahead of the tip, or tail end, of the cloud head. These winds are referred to as the sting at the end of the tail.

Fig.15 Weather-radar-network pictures showing the distribution of near-surface precipitation associated with two intense extra-tropical cyclones. (a): Cyclone centred over north-west Wales at 0300 UTC, 26 February 2002. (b): Cyclone just off the coast of north-east England at 0915 UTC, 30 October 2000. The approximate rain-rate key in (a) applies also to (b). Both cyclones had cloud heads with hooked tips. The second, more damaging, cyclone shows several curved bands of precipitation which terminate near Lincolnshire, near the tip of the cloud head. The first cyclone shows only one band of precipitation, which was associated with a rather broader hooked cloud-head, terminating just upwind of the Aberystwyth MST radar (A).

Fig. 16 Meteosat infra-red images for the two intense extra-tropical cyclones depicted in Fig.15. (a): Cyclone over north-west Wales, with cloud head over Ireland and cloud-head tip just west of Wales, at 0300 UTC, 26 February 2002. (b): Cyclone over the North Sea at 1200 UTC, 30 October 2000 (about 3 hours after Fig.15(b)) when the cyclone was close to its minimum central pressure. Multiple banding can be seen in (b) at the southern end of the cloud head close to the coast of north-east England.

Fig.17 Time-height sections of (a) wind speed (m s^{-1}) and (b) received power (dB) from 0000 to 0800 UTC, 26 February 2002, as obtained from the MST radar at Aberystwyth (A in Fig.15(a)) over which the tip of the cloud head passed shortly after 0300 UTC. (a) shows the cloud-head jet (CHJ) reaching 45 m s^{-1} in places below 4 km just after 0300 UTC. The black lines sketched in (a) correspond to axes of sloping maxima in received power in (b) which are believed to be indicative of the presence of multiple slantwise circulations in the cloud-head region.

Fig.18 Mesoscale model analyses for 1200 UTC, 30 0ctober 2000, showing the structure of the cyclone when its central pressure was close to its minimum:

(a) Mean-sea-level pressure, with isobars every 4 mb, and surface fronts inferred from (c). S and N represent the southern and northern ends of the cross-section along 2.5°E shown in Fig.19.

(b) Relative humidity, with respect to ice, at 500 mb, with isopleths at 10, 40 70 and 100% (shaded >100%).

(c) Absolute vorticity at 900 mb, with isopleths at 0,4,8 and $12x10^{-4}s^{-1}$ (shaded $> 4 \times 10^{4}s^{-1}$).

(d) Relative humidity at 800 mb, with isopleths at 40, 70 and 100% (shaded > 100%).

(e) Wet-bulb potential temperature at 900 mb, with isopleths at 1K intervals (shaded < 279K).

(f) Wind speed at 900 mb, with isotachs at 5 ms^{-1} intervals (shaded > 35 m s^{-1}). Dashed lines indicate axes of two low-level jets: one is associated with the warm conveyor belt ahead of the main cold front, and the other is the cloud-head jet associated with the cold conveyor belt near the southern end of the cloud head.

Fig.19 South-north cross-section (along SN in Fig. 18(a)) through the core of the cloud-head jet, obtained from mesoscale model analyses at 1200 UTC, 30 October 2000. (a): Wind speed, with isotachs every 5 m s^{-1} (shaded > 50 m s^{-1}). The label CHJ identifies the cloud-head jet. (b): Relative humidity with respect to ice, with isopleths at intervals of 30% above 10% (shaded > 100%). The 'cloud head' label in (b) denotes the northern part of the cloud head which then leaves

the cross-section to the west before re-entering it as a shallower feature, labelled cloud-head hook, beneath an intrusion of very dry, probably stratospheric, air.

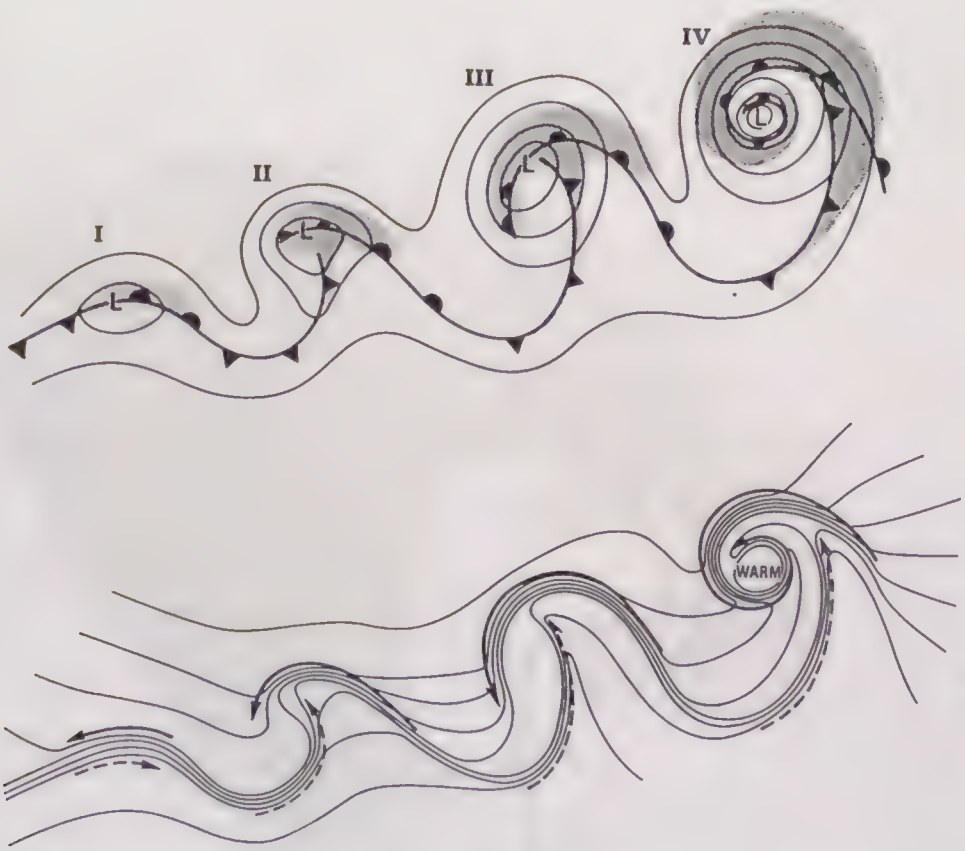

Fig. 1

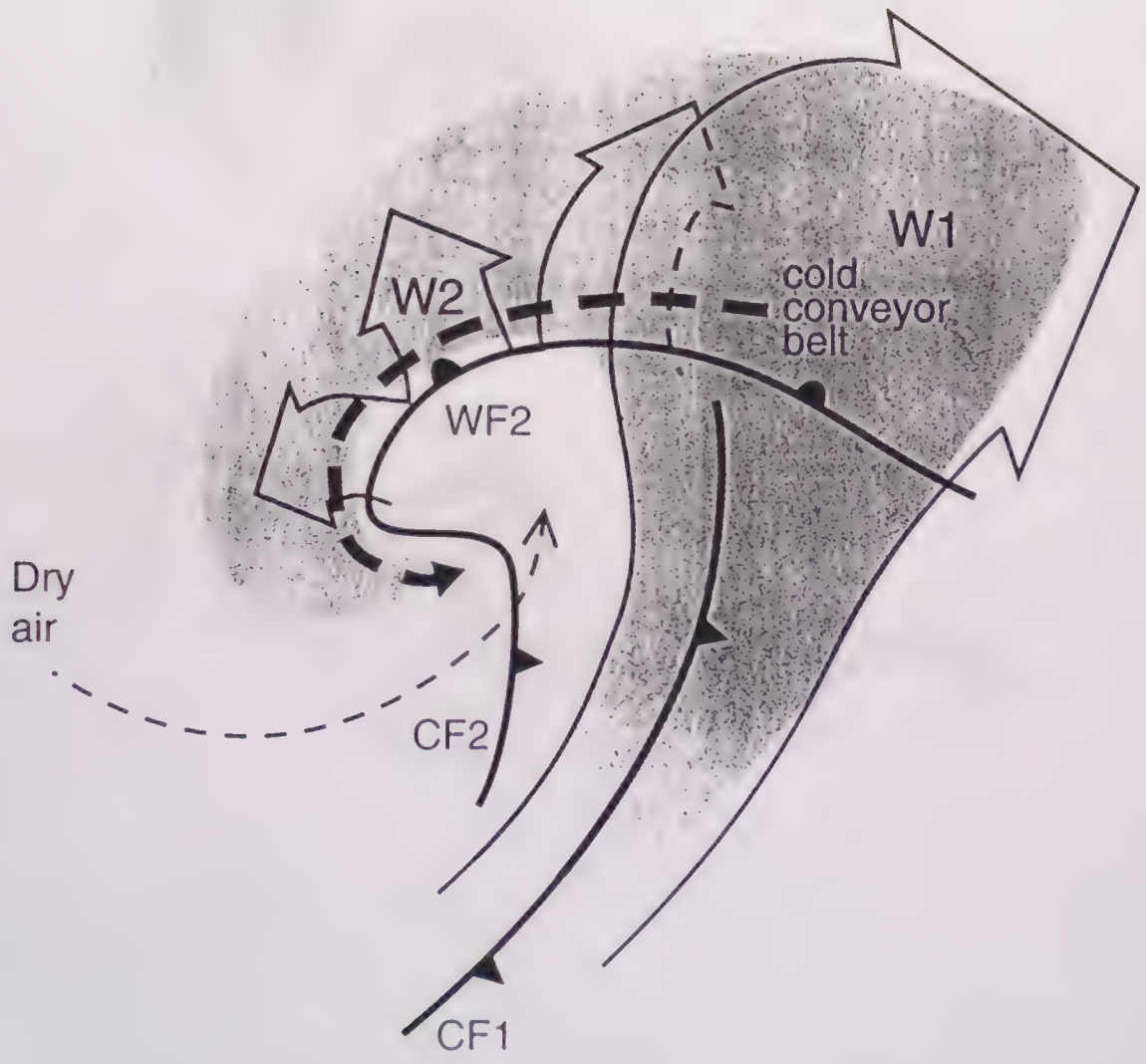

Fig. 2

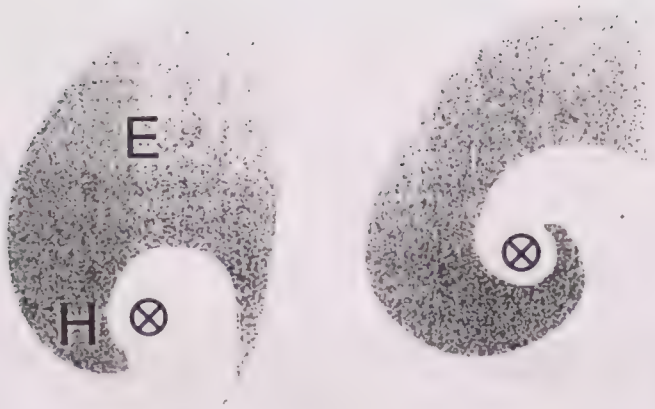

(a) Hook

(b) Hook moves forward of surface low

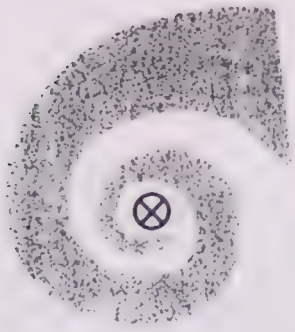

(c) Spiral

Fig 3

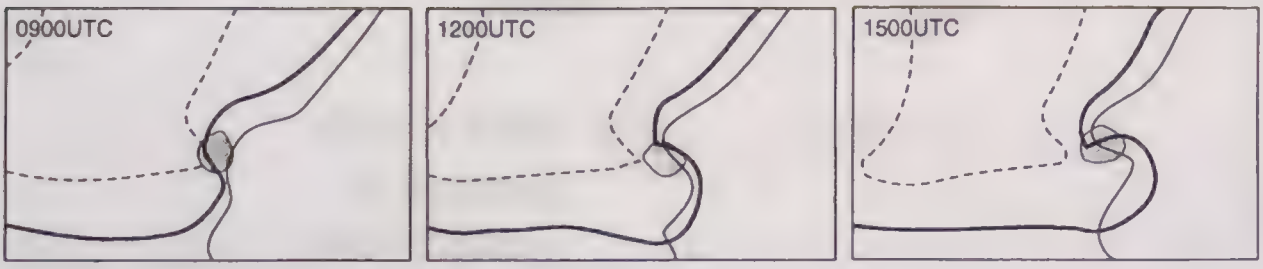

Fig 4

(a)

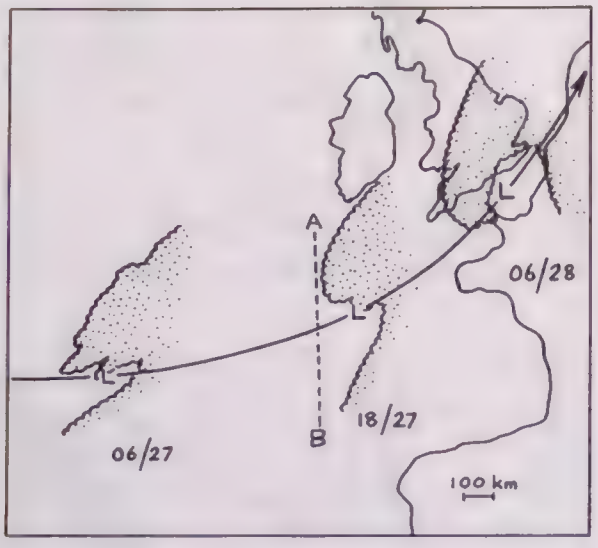

(b)

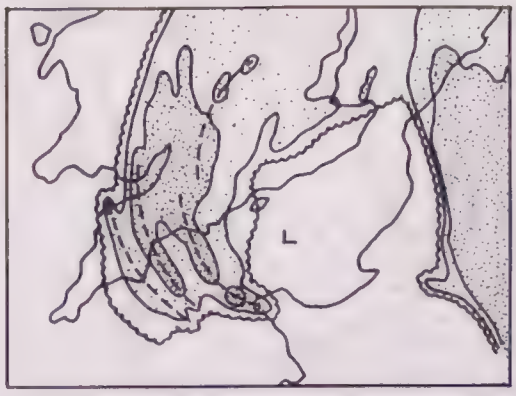

(c)

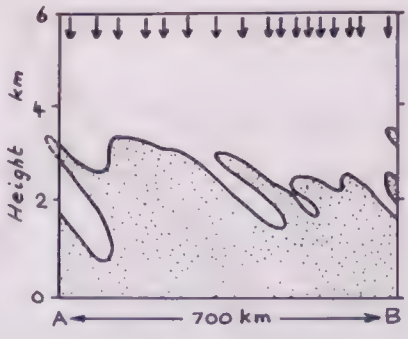

Fig 5

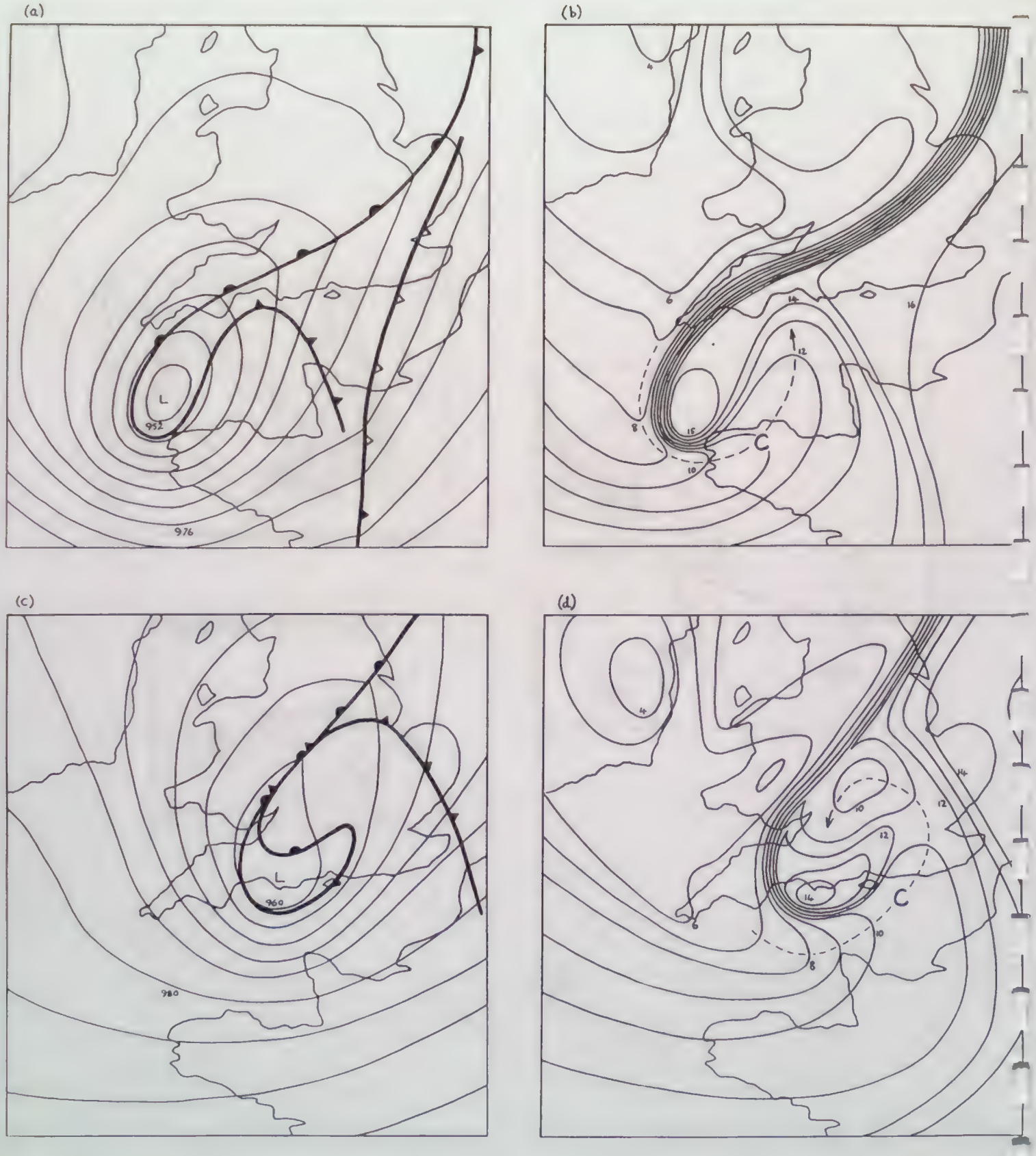

Fig 6

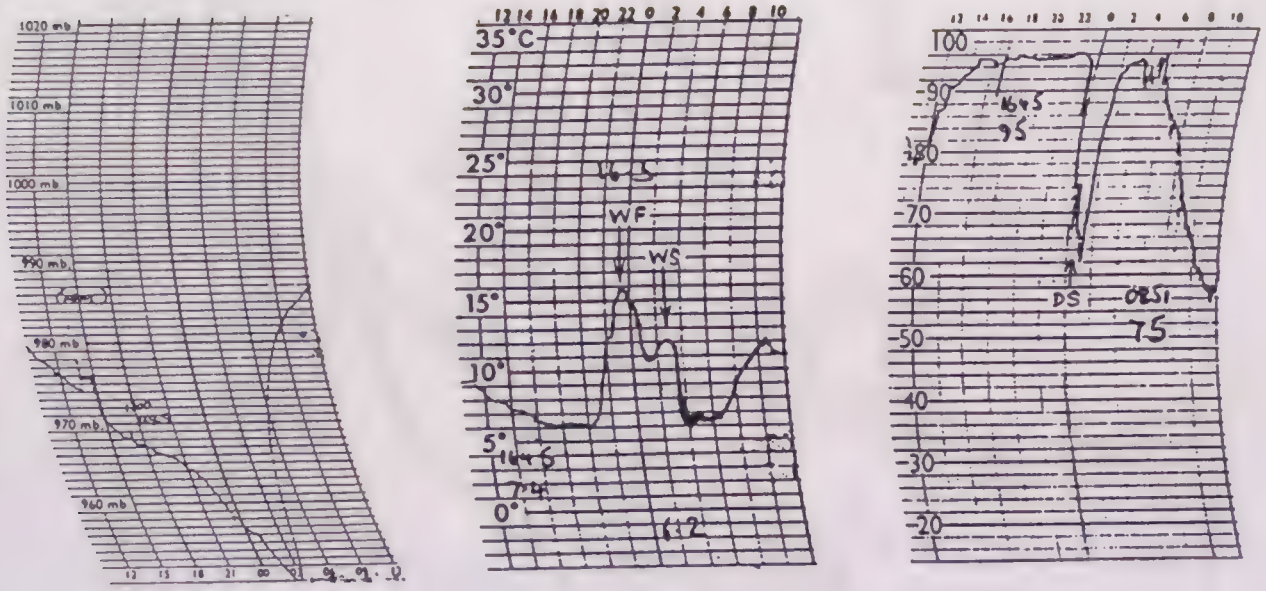
1020 mb
1010 mb
1000 mb
990 mb
980 mb
970 mb
960 mb
35°C
30°
25°
20°
15°
10°
5°
0°
WF
WS
DS
100
90
80
70
60
50
40
30
20
75

(a) (b) (c)

Fig 7

Fig 8

(a)

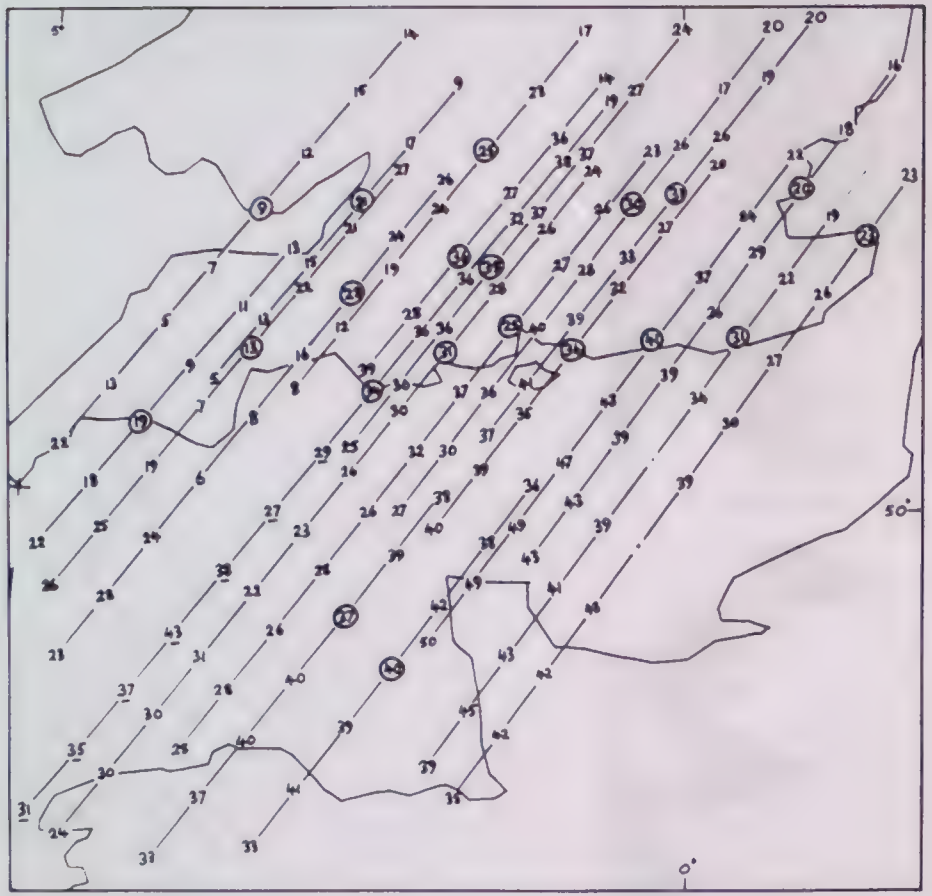

(b)

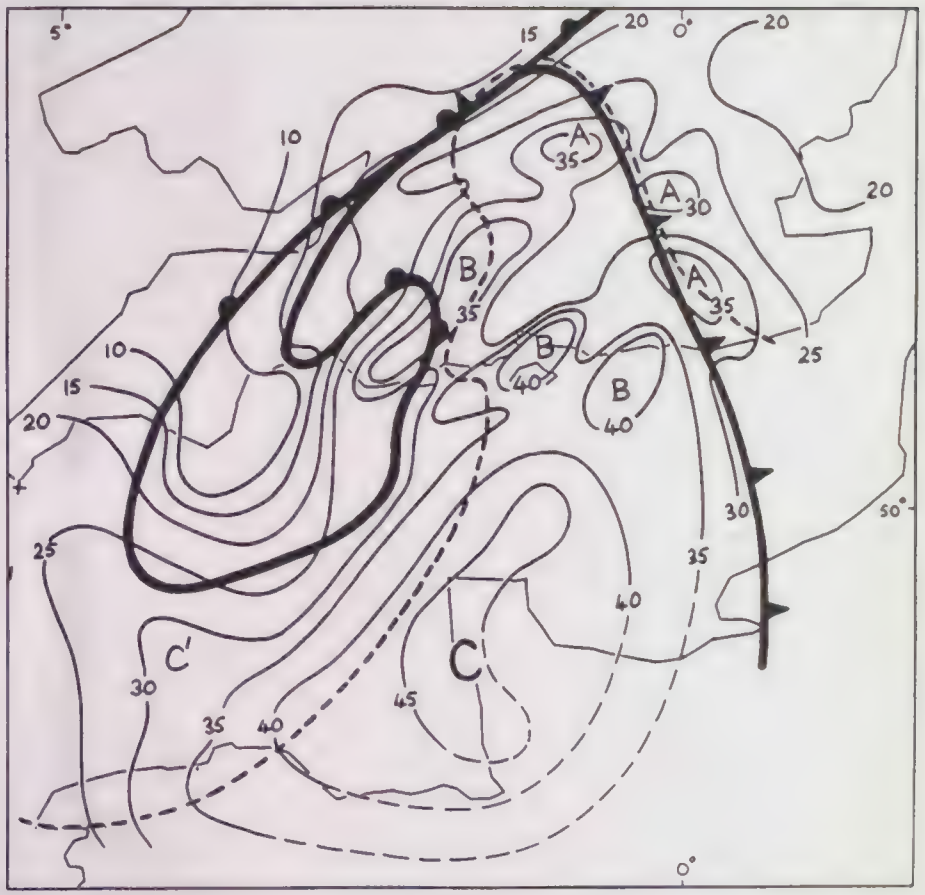

Fig.9

(a)

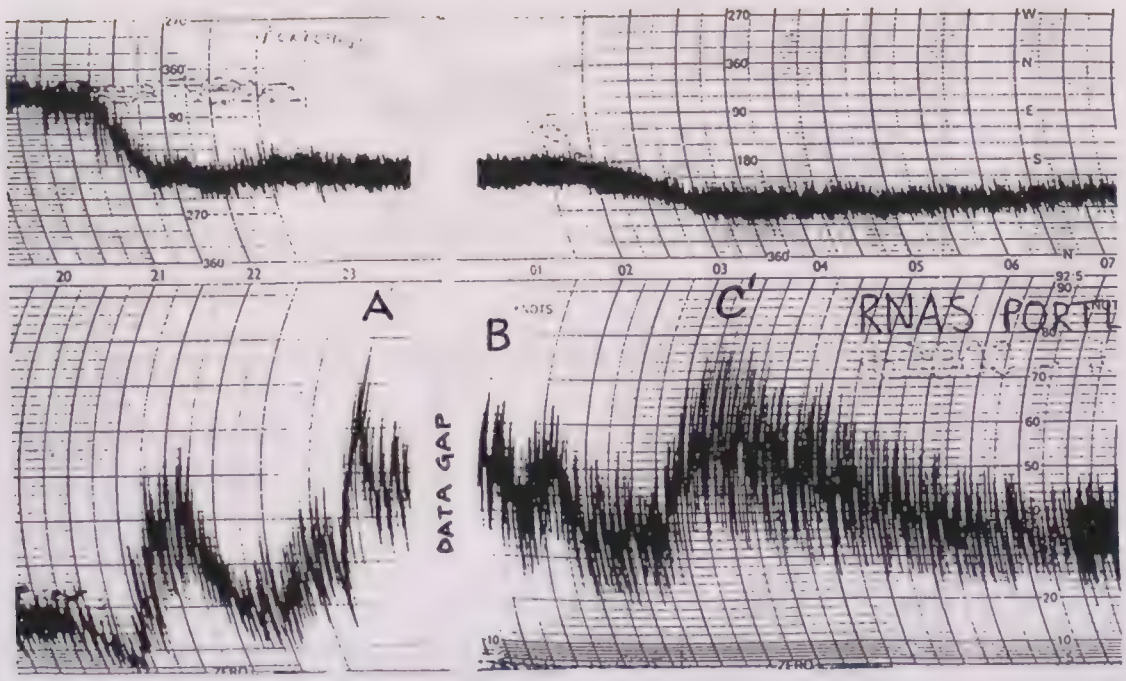

Fig 10 (a)

(b)

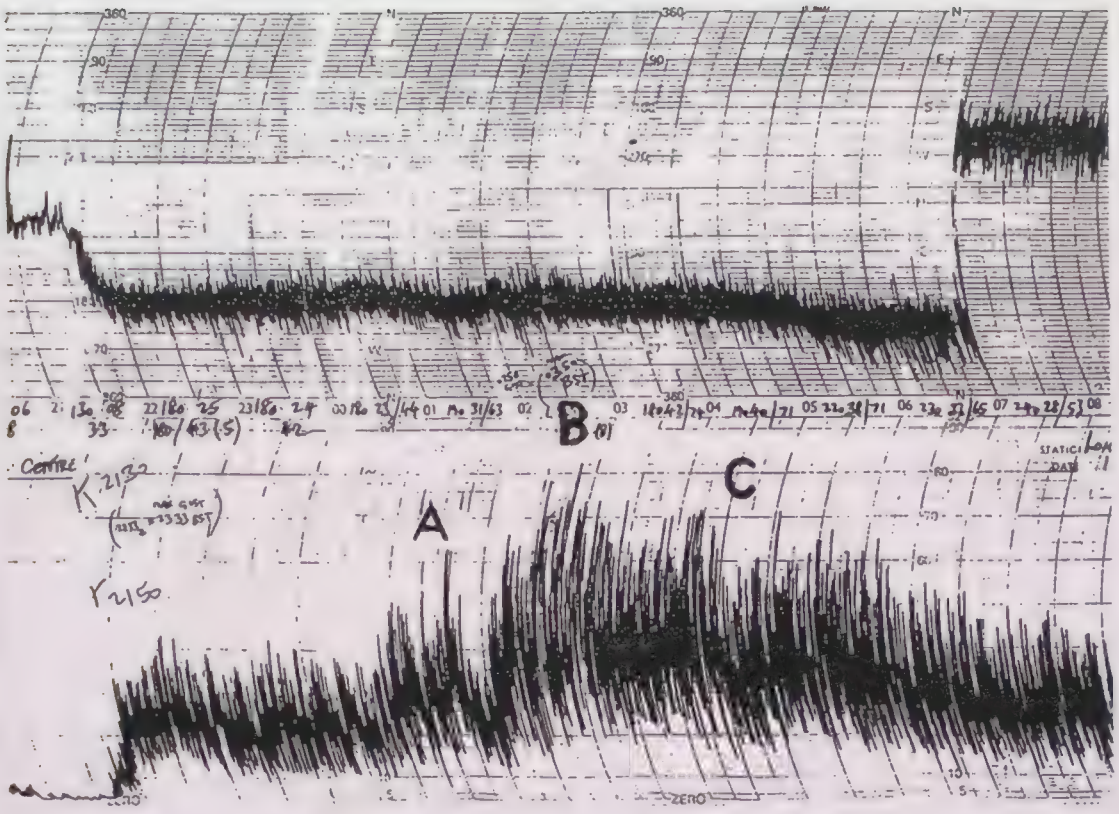

(c)

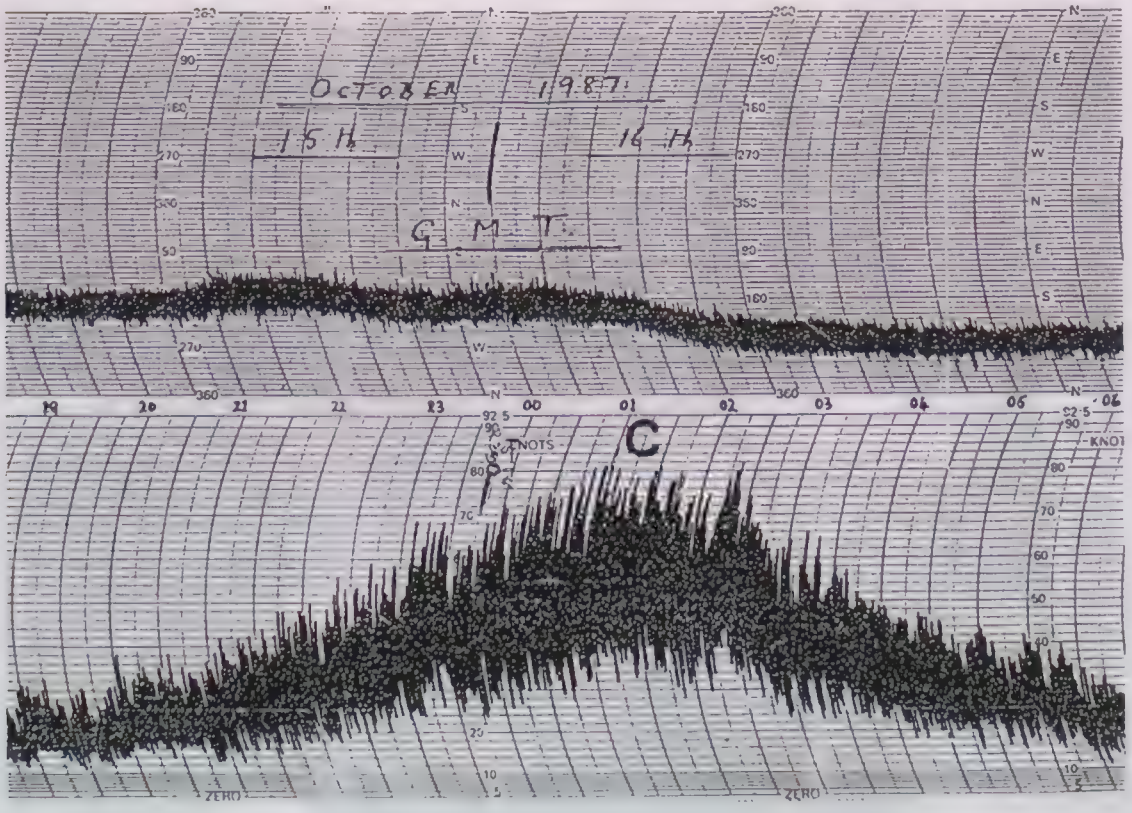

Fig 10

Fig. 11

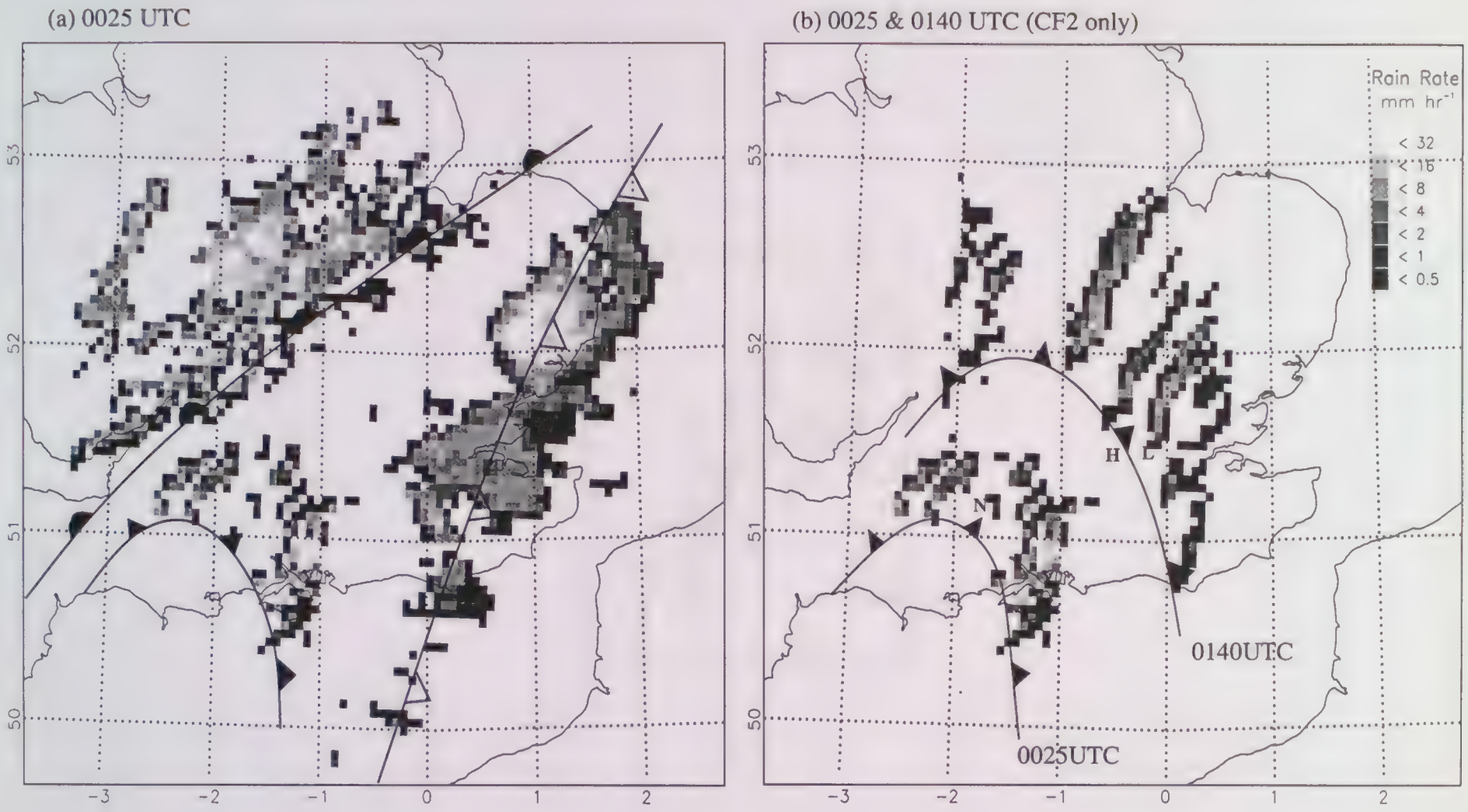
(a) 0025 UTC
(b) 0025 & 0140 UTC (CF2 only)
Rain Rate
mm hr-1
< 32
< 16
< 8
< 4
< 2
< 1
< 0.5
H
L
N
0140UTC
0025UTC
53
52
51
50
-3
-2
-1
0
1
2

Fig. 12

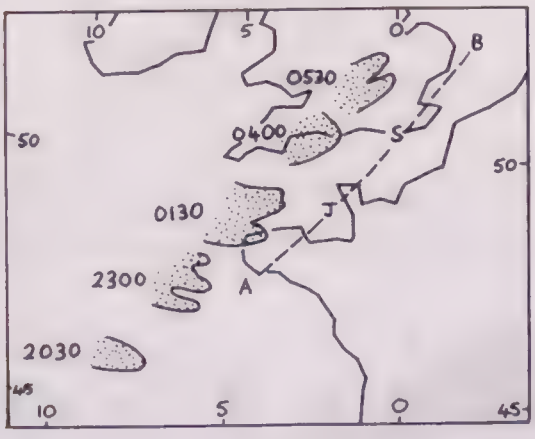

Fig. 13

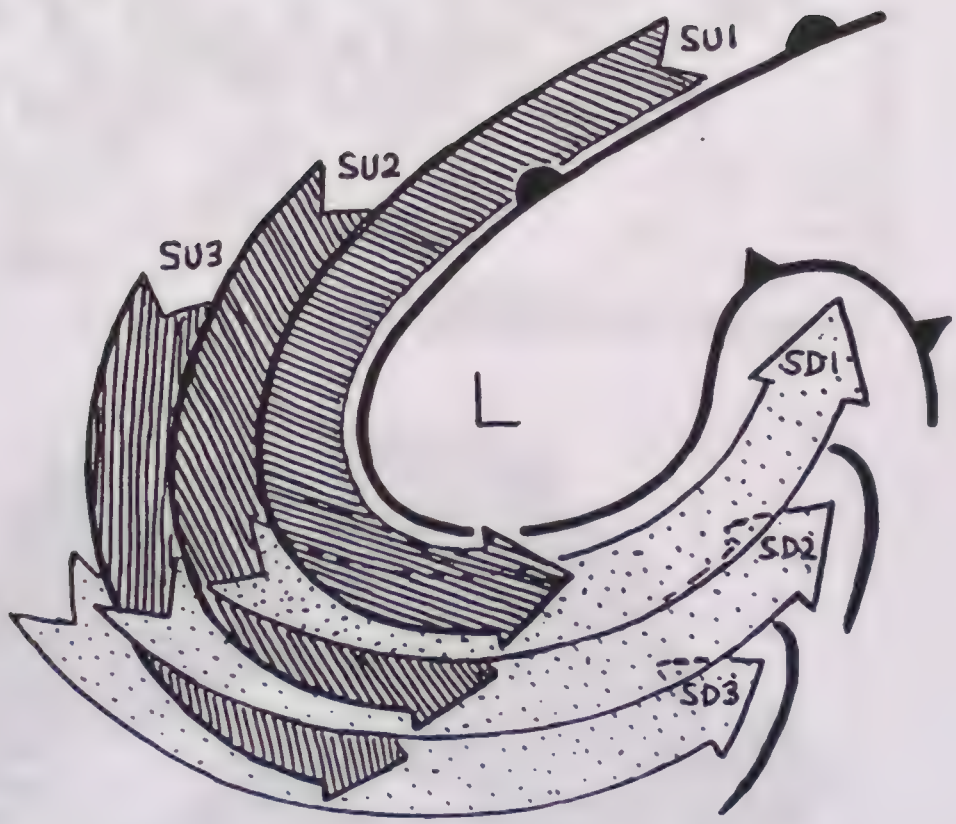

Fig 14

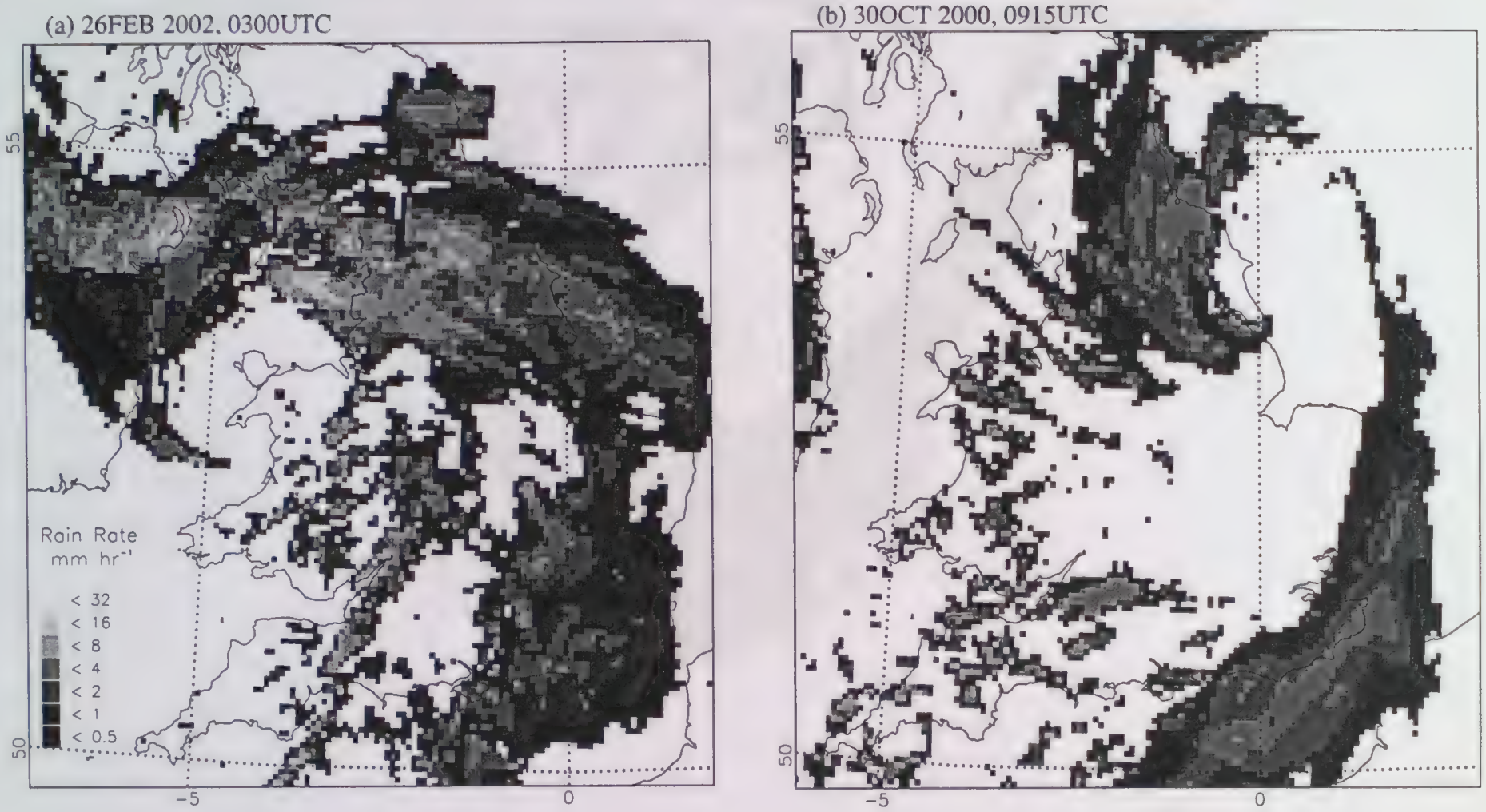
(a) 26FEB 2002, 0300UTC
(b) 30OCT 2000, 0915UTC
Rain Rate
mm hr-1
< 32
< 16
< 8
< 4
< 2
< 1
< 0.5
55
50
-5
0

Fig. 15

(a) 26FEB 2002, 0300UTC

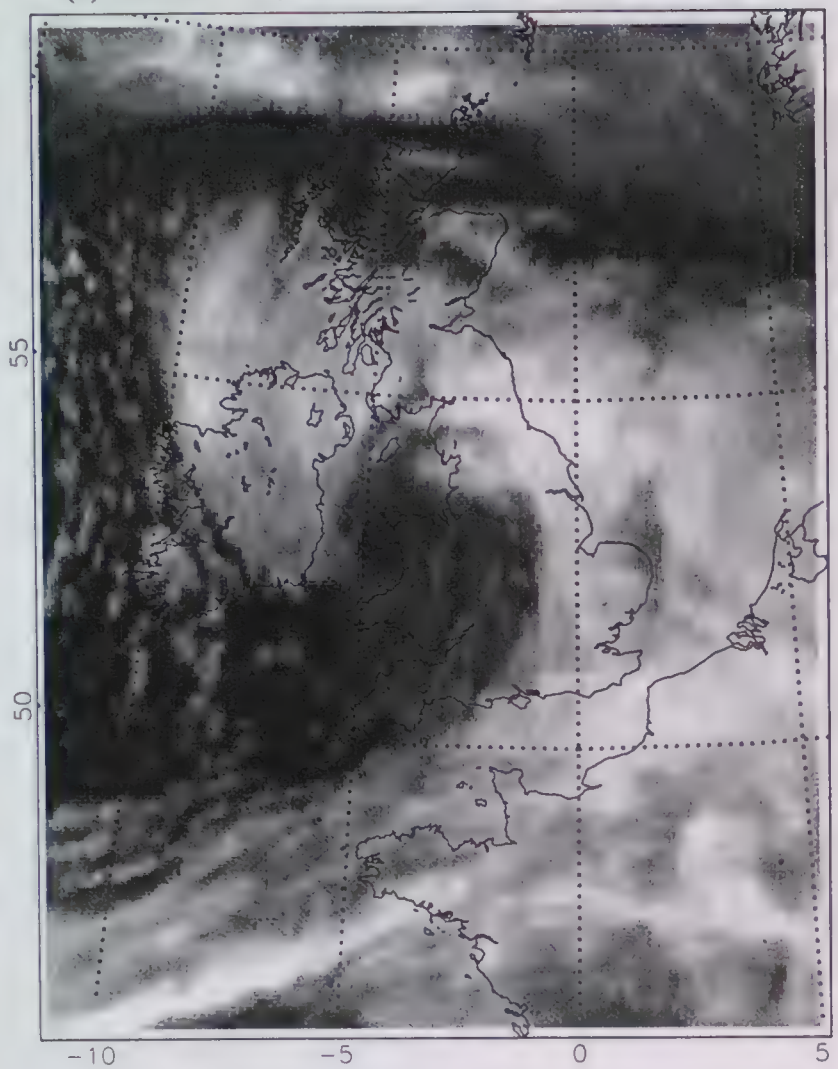

(b) 30OCT 2000, 1200UTC

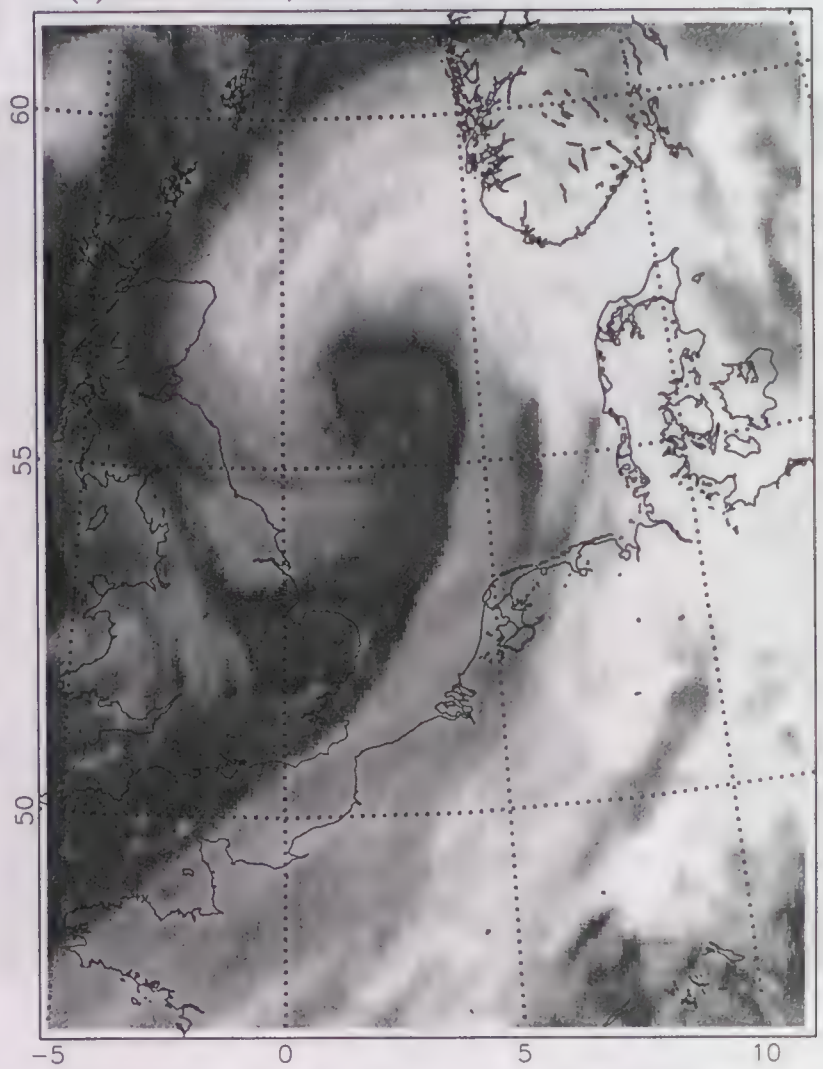

Fig. 16

(a) 26FEB 2002 Wind speed

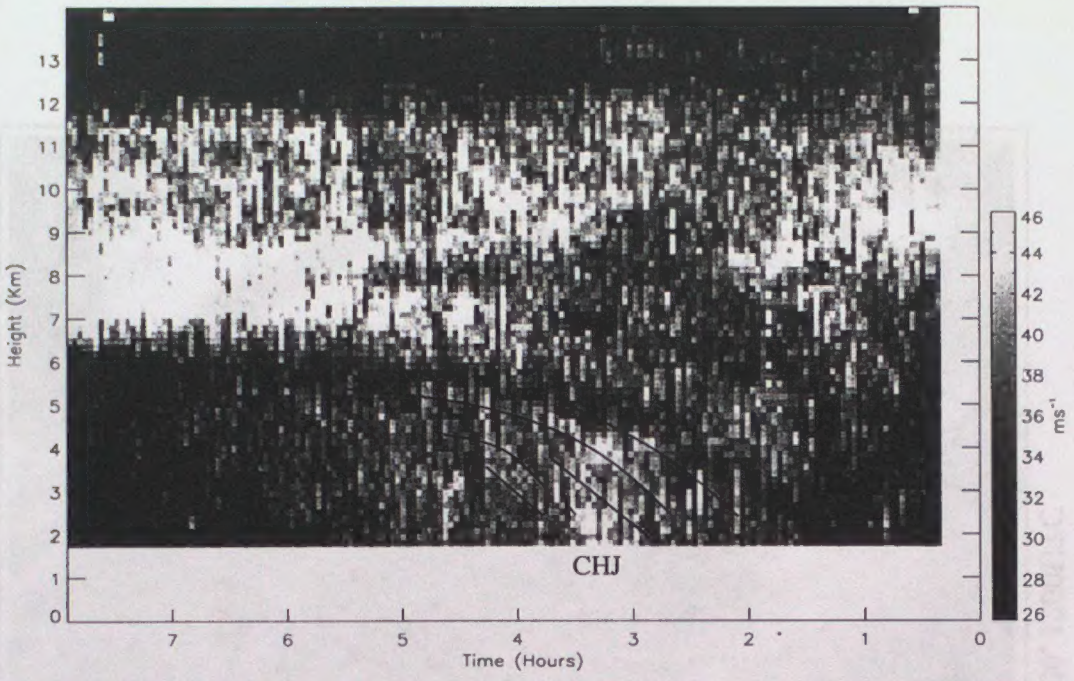

(b) 26 FEB 2002 Returned power

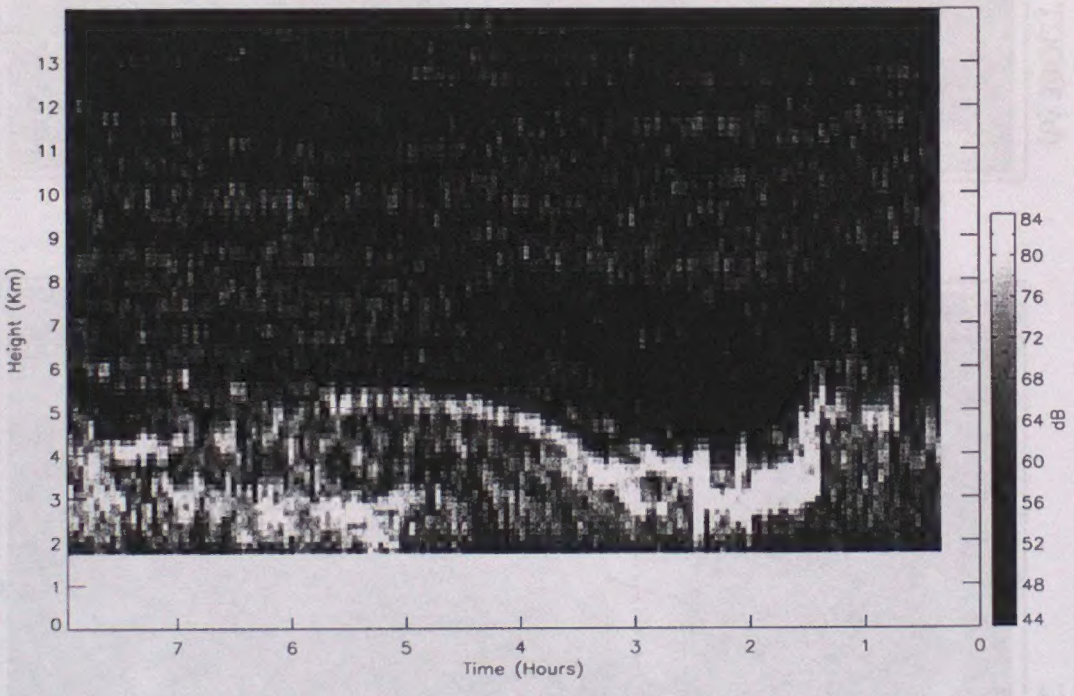

Fig 17

(a) MSLP

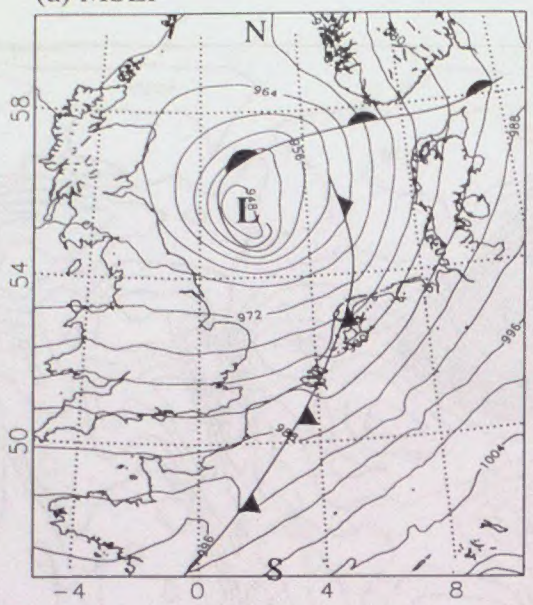

(b) RH at 500 mb

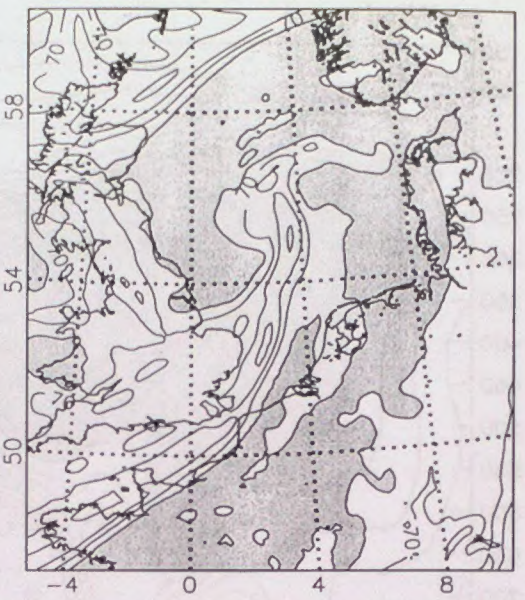

(c) Abs. vort. at 900 mb

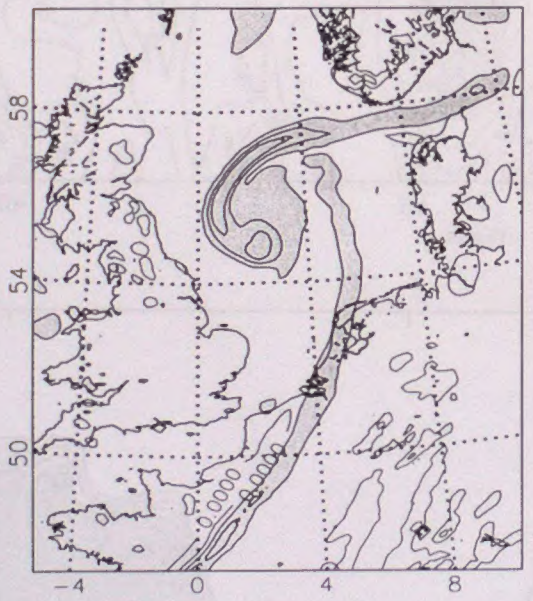

(d) RH at 800 mb

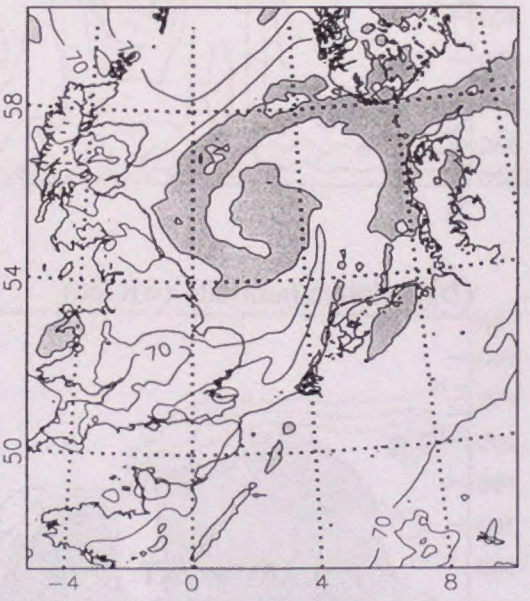

(e) Theta-W at 900 mb

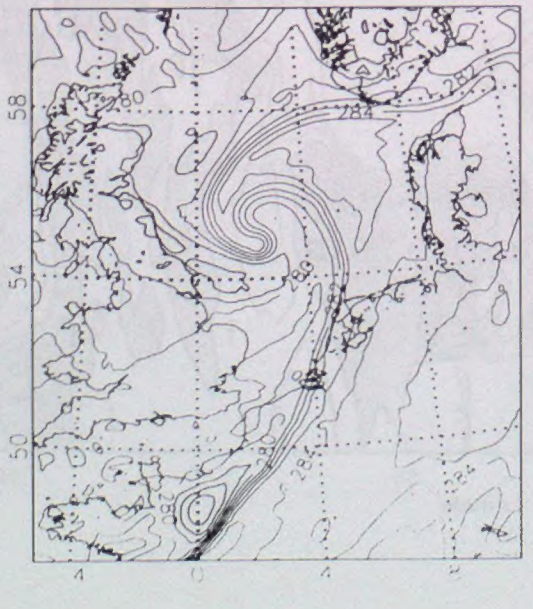

(f) Wind speed at 900 mb

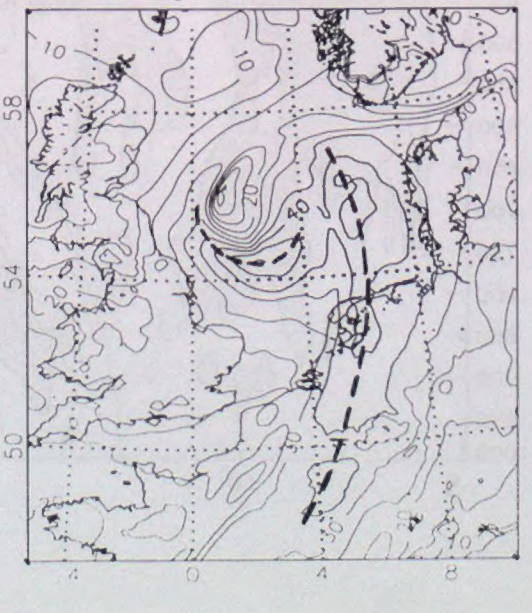

Fig. 18

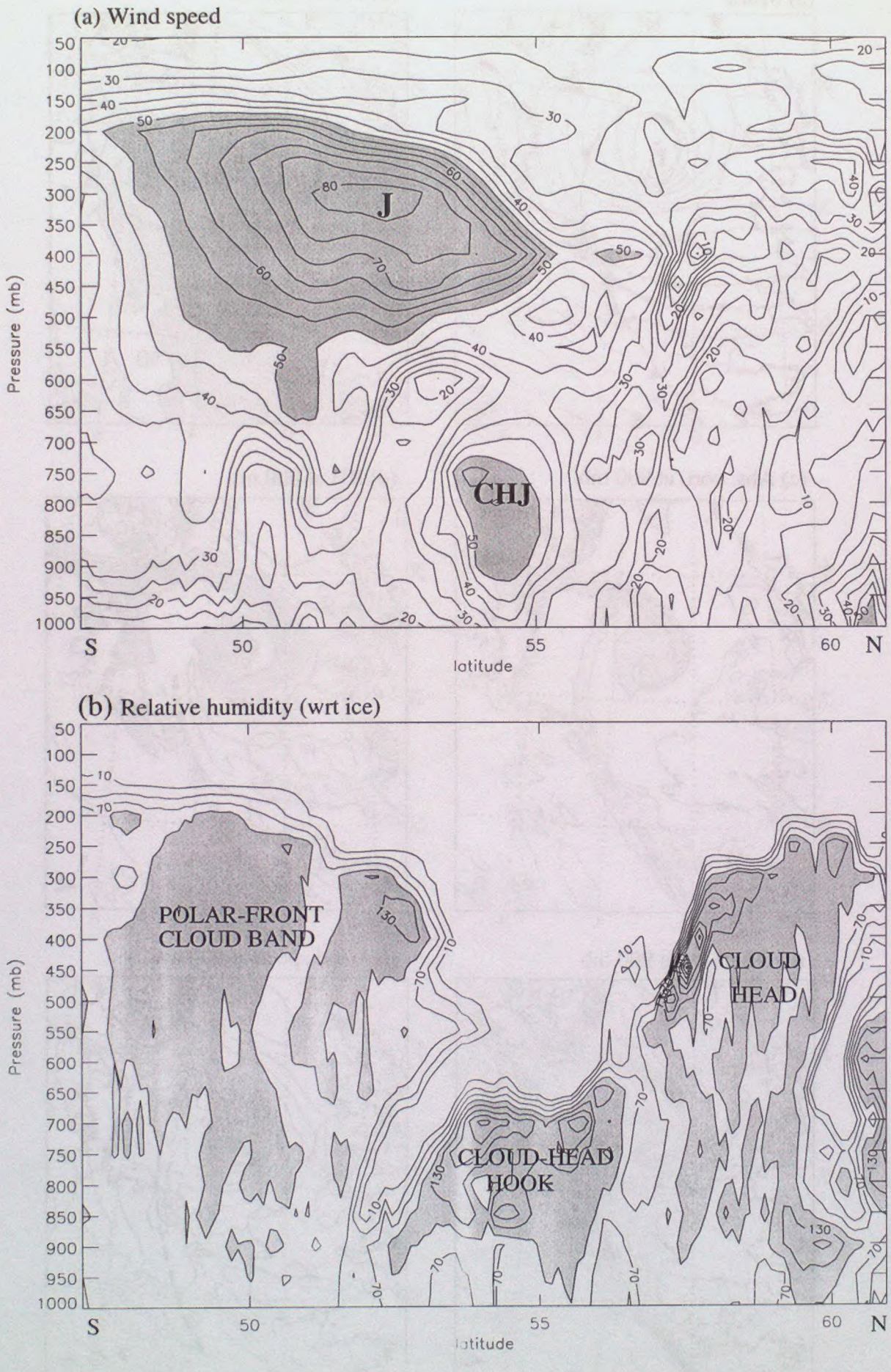
(a) Wind speed
Pressure (mb)
J
CHJ
S
50
55
60
N
latitude
(b) Relative humidity (wrt ice)
Pressure (mb)
POLAR-FRONT
CLOUD BAND
CLOUD
HEAD
CLOUD-HEAD
HOOK
S
50
55
60
N
latitude

Fig. 19